END-MEMBER MODELING OF SILICICLASTIC GRAIN-SIZE DISTRIBUTIONS: THE LATE QUATERNARY RECORD OF EOLIAN AND FLUVIAL SEDIMENT SUPPLY TO THE ARABIAN SEA AND ITS PALEOCLIMATIC SIGNIFICANCE

MAARTEN A. PRINS
Department of Geology, Faculty of Earth Sciences, Utrecht University, P.O. Box 80021, NL-3508 TA Utrecht, The Netherlands; e-mail: mprins@geo.uu.nl
AND
GERT JAN WELTJE
Department of Geology, Faculty of Earth Sciences, Utrecht University, P.O. Box 80021, NL-3508 TA Utrecht, The Netherlands
Present addresses: Department of Geo-Energy, Netherlands Institute of Applied Geoscience TNO, P.O. Box 6012, NL-2600 JA Delft, The Netherlands; e-mail: g.weltje@nitg.tno.nl and Subfaculty of Applied Earth Sciences, Delft University of Technology, P.O. Box 5028, NL-2600 GA Delft, The Netherlands; e-mail: g.j.weltje@ta.tudelft.nl

ABSTRACT: Numerical-statistical algorithms are used to model end-member grain-size distributions of pelagic and hemipelagic siliciclastic sediments of the Arabian Sea. The grain-size distributions of sediments from the Oman continental slope, the Owen Ridge, the Pakistan continental slope, and the Indus Fan can be adequately described as mixtures of three end members. The spatial variation in relative contribution of the end members is interpreted in terms of transport processes and provenance. In the western Arabian Sea, deposition is dominated by two end members that represent "proximal" and "distal" eolian dust. A third end member, which dominates the deposits of the middle Indus Fan, represents fluvial mud deposited from low-density turbidity currents (lutite flows).

At any given location, the temporal changes in the relative contribution of the end members can be interpreted in terms of climate change. The ratio of contributions of the two eolian end members (i.e., the grain-size distribution of the eolian dust) on the Owen Ridge (NIOP492) reflects the strength of the summer monsoon. Deposition on the upper Indus Fan (NIOP458) is dominated by "distal" eolian dust and fluvial mud. The ratio of contributions of eolian and fluvial sediment reflects continental aridity. The ratio of contributions of the two eolian end members (i.e., the grain-size distribution of the eolian dust) on the upper Indus Fan reflects the strength of the winter monsoon.

Our reconstruction of the late Quaternary variations in Arabian Sea monsoon climate corresponds well with interpretations of the loess-paleosol sequences on the Chinese Loess Plateau. In both areas, the bulk of the annual precipitation is confined to the summer monsoon season. Intensification of the summer monsoon during interglacials, which has been identified as the principal control on pedogenesis on the Loess Plateau, also explains increased discharge of Indus River-derived muds to the northern Arabian Sea. Independent evidence for summer monsoon strength, provided by the eolian grain-size record of the western Arabian Sea, fully supports this conclusion. The strength of the summer monsoon thus provides an aridity forcing mechanism for both the Arabian Sea and the Loess Plateau. The grain size of the eolian dust in the northern Arabian Sea and on the Loess Plateau indicates intensified winter monsoons during glacials.

INTRODUCTION

Cores of late Quaternary deep-sea sediments provide continuous records that can be dated accurately. The terrigenous fraction of deep-sea sediments reflects the supply of sediments produced on the continents surrounding the basin. Such records potentially hold the key to reconstructing paleoclimatic evolution over geological time spans. In many cases, deep-sea siliciclastics are mixtures of a pelagic component brought in by the wind and a hemipelagic component supplied from the shelf by low-density turbidity currents. Hemipelagic sediment escaping from shelves by transport in semipermanent currents (exemplified by the plumes seen off deltas) is mainly deposited on the slope and rise. Volumetrically less important are wave- and current-induced transport of sediments across the shelf. Most of the hemipelagic material is ultimately derived from fluvial sources, and is stored in cones and fans off the major river deltas (McCave, 1972). The flux of river-derived fine-grained siliciclastics is expected to correlate with continental runoff, and thus provides a proxy for continental humidity. Analysis of eolian dust allows estimation of the past aridity of eolian source regions, via flux determinations, and of the intensity of the transporting winds, via grain-size measurements. These two parameters, the grain size and the mass flux of eolian dust, may vary independently (Rea, 1994). Clearly, the source of the sediments must be known before variations within the terrigenous fraction can be interpreted in terms of changes in paleoclimate.

Successful reconstructions of paleoclimate from siliciclastic deep-sea records depend primarily on the capability of distinguishing between sediments of eolian and fluvial origin. In certain cases, use can be made of a priori knowledge of the provenance and dispersal patterns to distinguish the two types of sediment input. For instance, Rea and Hovan (1995) characterized the size distribution of "typical" eolian dust and hemipelagic mud in the abyssal Pacific Ocean by selecting "end-member samples" based on independent evidence. Eolian samples were selected from slowly accumulating pelagic clays deposited far from land and downwind from the Chinese Loess Plateau. The mineralogy and chemical composition of the samples were identical to the composition of "local" atmospheric dust and Chinese loess. Hemipelagic mud samples were selected from sites closer to the shore in settings characterized by moderate to high accumulation rates. Their mineralogy and chemical composition were identical to the composition of adjacent continental-margin sediments of presumed fluvial origin. Both types of "end-member samples" have modes around 2 μm, but differ strongly in the extent of sorting. Rea and Hovan (1995) argued that the small grain size of the eolian dust in the Pacific Ocean is the result of the distant location of the source area, the Chinese Loess Plateau. Eolian dust deposited closer to the source area is much coarser, as shown by Koopmann (1981) and Sarnthein et al. (1981, 1982) off northwest Africa, and by Sirocko (1991) and Sirocko et al. (1991) off the Arabian peninsula. Because marine sediments deposited close to an eolian source are likely to be mixtures of eolian dust and hemipelagic mud, Koopmann (1981), Sarnthein et al. (1981, 1982), and Sirocko et al. (1991) used a somewhat arbitrary cutoff of 6 μm to partition eolian and hemipelagic sediments. They considered the fraction coarser than 6 μm to be of predominantly eolian origin, and the fraction smaller than 6 μm to be of fluvial origin (hemipelagic mud).

Numerical Experiments in Stratigraphy: Recent Advances in Stratigraphic and Sedimentologic Computer Simulations, SEPM Special Publications No. 63,

In many geological applications of grain-size analysis, no a priori knowledge is available to distinguish subpopulations of sediments with different provenances. Indeed, reconstruction of provenance and dispersal patterns is the objective of most studies. The best way to proceed in such cases would be to use an inverse method that does not require detailed assumptions about the geological system being studied. In this study, an inversion algorithm for end-member modeling of compositional data (Weltje, 1994, 1997a), developed for "unmixing" of multisourced basin fills in the absence of prior knowledge, is applied to a large data set of grain-size distributions of siliciclastics from the Arabian Sea (northwest Indian Ocean). Our objectives are to (1) unravel late Quaternary deep-sea records of fine-grained siliciclastics that were supplied by multiple sources, and (2) demonstrate that the reconstructed fluxes and grain-size distributions of the sediments shed by each source provide valuable information about the paleoclimatic evolution of the surrounding continental areas.

Previous Methods Developed for Discrimination of Grain-Size Subpopulations

Parametric approaches.—

Doeglas and Brezesinska Smithuysen (1941) and Doeglas (1946) observed that many cumulative grain-size distributions drawn on arithmetic probability paper appear to be composed of two or more practically straight line segments. They argued that such curves are caused by the mixing of materials of different origins, which possess Gaussian (normal) distributions. Visher (1969) followed a similar line of reasoning by stating that grain-size distributions do not follow a simple log-normal law, but are composed of several log-normal subpopulations, each with a different mean and standard deviation. He distinguished at least three subpopulations produced by three modes of sediment transport: surface creep/rolling, saltation, and suspension. A theoretical basis for the existence of different transport populations was provided by the hydraulic models of Middleton (1976) and Bridge (1981). Curray (1960) plotted grain-size distributions on a logarithmic scale (ϕ units) and manually decomposed polymodal frequency distributions into a series of Gaussian (log-normal) distributions. An automated version of Curray's method was developed by Sheridan et al. (1987).

The sequential fragmentation transport (SFT) theory of Wohletz et al. (1989) is another parametric method for interpretation of polymodal grain-size distributions. This theory is based on the assumption that observed grain-size distributions have been produced by a sequence of repeated steps of breakage and selective transport, represented by a series of SFT subpopulations with variable skewness. Decomposition into unimodal SFT distributions has been applied to volcanic ash and pyroclastic grain-size distributions by Wohletz et al. (1989) and Lirer et al. (1996).

All of these methods are parametric in the sense that they require a priori specification of the end-member grain-size distributions. This may not be desirable in many cases in view of our incomplete understanding of the mechanisms governing the grain-size distribution of natural sediments. In the worst case, such a parametric approach could even hamper the recognition of subpopulations with size distributions differing markedly from the adopted model (Gaussian, log-Gaussian, or SFT). The existence of subpopulations that do not fit one of the theoretical grain-size distributions is likely in view of the potentially unlimited number of combinations of initial and acquired characteristics of sediments (e.g., parent material, weathering history, mode of transport). Another disadvantage of these methods is that the decomposition is performed on individual grain-size distributions. The information contained in the covariance structure of the data is not used at all. Large data sets cannot be easily analyzed with any of these techniques, as exemplified by Curray (1960), who manually formed groups of subpopulations with similar modes in order to simplify the results of his analysis.

Nonparametric approaches.—

A different view on grain-size distributions is to regard the proportion of mass in each size class as an attribute of a multivariate measurement; i.e., to consider each grain-size distribution as consisting of as many components as there are size classes. Proportions of mass in two or more size classes may be negatively or positively correlated across a series of grain-size distributions. Such variation among individual measurements is contained in the covariance structure of a data set. The nonparametric methods discussed in the following sections all make use of this source of information to group samples with similar overall characteristics. In contrast with the previous methods, the functional forms of the groups, clusters, or end members do not have to be specified a priori. Nonparametric approaches to the recognition of subpopulations in grain-size data include methods such as cluster analysis (Zhou et al., 1991) and multivariate entropy analysis (Forrest and Clark, 1989); however, the family of multivariate techniques used most extensively for this purpose comprises principal component analysis (e.g., Davis, 1970; Chambers and Upchurch, 1979; Lirer and Vinci, 1991; Zhou et al., 1991) and factor analysis (e.g., Klovan, 1966; Solohub and Klovan, 1970; Allen et al., 1971, 1972; Dal Cin, 1976; Sarnthein et al., 1981; Syvitski, 1991).

The aim of principal component analysis (PCA) and factor analysis (FA) is to decompose the data matrix into two matrices: (1) a matrix of "components" or "factors" from which inferences may be drawn about the shapes of the grain-size distributions of each of the groups recognized in the data, and (2) a matrix representing the extent to which each of the input grain-size distributions matches each of these components or factors (Jöreskog et al., 1976; Davis, 1986). Thus, interpretation of the subpopulations is based on the properties of the first matrix, and classification of the observations is based on the properties of the second matrix. A major problem with both techniques is that the units in which the output is cast are difficult to interpret because they cannot be expressed in physical terms (for instance, a typical input variable for grain-size analysis, a weight proportion, may have been "miraculously" transformed to a negative value in a component or factor matrix). This is unfortunate because the predominant application of PCA and FA in sedimentology has been in the field of unmixing polymodal grain-size distributions.

Specialist techniques are required if the analytical objective is to unravel grain-size distributions subject to strict physicality (i.e., non-negativity and constant sum) constraints. End-member modeling algorithms are aimed at construction of physical mixing models that express the input data as mixtures (non-negative contributions) of a limited number of end members with realistic (i.e., non-negative) compositions. The techniques of Klovan and Miesch (1976), Full et al. (1981, 1982), Renner (1993, 1995), and Weltje (1994, 1997a) have been developed with this objective in mind. Fillon and Full (1984) and Wohletz et al. (1989) applied the techniques of Full et al. (1981, 1982) to grain-size-distribution data. In both cases, the modeled end members have varying skewness and are of no simple mathematical form, supporting the idea that parametric decomposition into predefined end members may not be the best approach toward an understanding of variation among grain-size distributions.

The end-member modeling algorithm of Weltje (1994, 1997a) has been tested on petrographic data of modern beach sands to evaluate its usefulness for unraveling multisourced basin fills in the absence of prior knowledge (Weltje, 1995). Experiments with artificial sediment mixtures (Prins and Weltje, unpublished data) indicate that the algorithm successfully estimates mixing proportions and end-member grain-size distributions in the absence of prior knowledge. Van Dam and Weltje (in press) applied the algorithm to Miocene rodent associations in southwestern Europe to reconstruct continental paleoclimate variations. A brief summary of the end-member modeling technique of Weltje (1994, 1997a) is given in the material and methods section.

The Arabian Sea

Regional setting.—

The Arabian Sea constitutes the northwestern Indian Ocean and is enclosed by the Somalian and Arabian peninsulas in the west, Iran and Pakistan in the north, and the Indian peninsula in the east (Figure 1). The most conspicuous geological feature in the Arabian Sea is the Indus Fan, which occupies the complete central part of the basin. The Indus Fan, with a length of 1600 km and a maximum width of 1000 km, covers an area of approximately 1.1–1.25 million km^2 (McHargue and Webb, 1986; Kolla and Coumes, 1987). It is the second-largest deep-sea fan in the world. The fan developed off the passive continental margin of Pakistan-India, and is bounded by the Chagos-Laccadive Ridge in the east, by the Owen-Murray Ridges in the west, and in the south by the Carlsberg Ridge, which is a portion of the Central Indian Ridge (mid-ocean ridge).

Monsoon-driven sedimentation patterns.—

The Indian Ocean monsoon winds are driven by strong differential heating between the Indian Ocean and the Indian-Asian continents, and by the availability of vast amounts of latent heat collected over the southern hemisphere Indian Ocean; this heat is released over the high elevations of the Indian-Asian landmasses, the area of monsoon precipitation. Differential heating during the northern hemisphere winter causes low surface pressure over the southern Indian Ocean and high surface pressure over the high elevations of the Indian-Asian continents. This northeast-southwest pressure gradient is responsible for driving the winter monsoon circulation, which results in relatively weak northeastern monsoon winds over the Arabian Sea. During spring, when the Indian-Asian continents start to heat up, west–northwest winds prevail over the Arabian Sea. During peak summer, strong southwest monsoon winds develop when the continents become warmer than the oceans and the pressure gradient reverses (Clemens and Prell, 1990; Clemens et al., 1991; Sirocko, 1991).

At present, the monsoon climate strongly influences sedimentation processes within the Arabian Sea. The northwesterly winds are responsible for the transport of large quantities of eolian dust from the Arabian peninsula, and minor amounts from Pakistan. The southwest monsoon winds supply minor amounts of eolian dust originating from Somalia. The northeast monsoon winds transport minor amounts of eolian dust from Pakistan and northern India (e.g., from

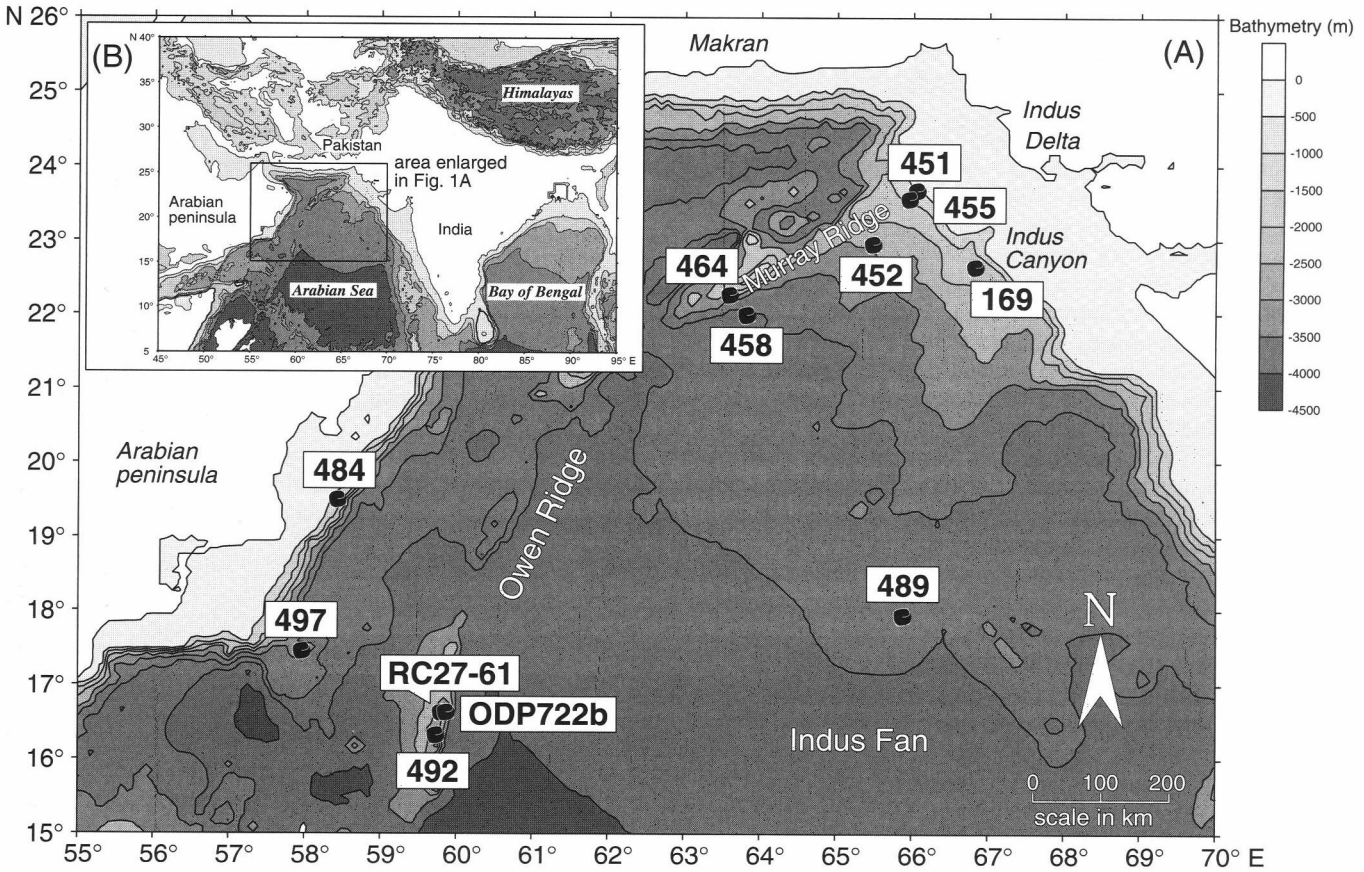

FIG. 1.—Topographic maps of the Arabian Sea and adjacent landmasses. (A) Study area with location of cores. Contour interval 500 m. (B) Inset map shows location of study area. Contour interval 1000 m. Topographic data from U.S. National Geophysical Data Center/World Data Center A for Marine Geology and Geophysics.

the Thar desert) toward the Arabian Sea (Sirocko, 1991). Annually, 115–215 million tons of eolian dust is transported from adjacent continents to the Arabian Sea (Sirocko and Sarnthein, 1989).

The southwest monsoon carries large amounts of water vapor that is released as precipitation over the Indian-Asian continent. This precipitation provides the runoff for river systems draining the Himalayas, including the Indus River, which flows into the Arabian Sea. Before the Indus River was effectively dammed and channeled, which resulted in almost complete cessation of water and sediment discharge, the river was one of the world's largest in terms of both discharge and sediment load. Before dam construction, somewhat less than 250 million tons of suspended sediment reached the Indus Delta annually (Milliman et al., 1982). Highest discharge coincides with the peak of the rainy season (July), and up to 80% of the annual cumulative discharge occurs during the southwest monsoon summer season (Beg, 1977).

The monsoons cause seasonal reversals in surface circulation of the Arabian Sea, resulting in upwelling of nutrient-rich water along the coasts. Nair et al. (1989) recorded strong seasonality in particle flux at three sediment trap sites (western, central, and eastern Arabian Sea) with peaks during the southwest and northeast monsoons. High primary productivity during the monsoons resulting from wind-induced mixed-layer deepening and the associated nutrient injection into the euphotic zone appeared to be the main factor controlling the observed particle flux pattern. Highest terrigenous particle fluxes are recorded during the southwest monsoon season. At the western sediment trap site, 80% of the annual cumulative terrigenous particle flux is recorded during this season. Because the western trap site is close to the Arabian peninsula, deposition is dominated by eolian dust blown in from the Arabian deserts. At the eastern site, 67% of the annual cumulative terrigenous particle flux is recorded during the summer season, and it is dominated by input of Indus River muds.

Eolian records.—

During the last decade many studies concerning the marine sediment record in the Arabian Sea have concentrated on the faunal response to wind-induced upwelling (e.g., Clemens and Prell, 1990; Shimmield et al., 1990; Murray and Prell, 1991; Shimmield and Mowbray, 1991; Reichart et al., 1998) and on eolian dust transport in relation to the monsoon climate (e.g., Sirocko and Sarnthein, 1989; Clemens and Prell, 1990, 1991; Clemens et al., 1991; Krissek and Clemens, 1991; Sirocko, 1991; Sirocko and Lange, 1991; Sirocko et al., 1991, 1993; Reichart et al., 1998).

Sirocko (1991) and Sirocko et al. (1991) used the percentage of sediment in the size fractions greater than 20 μm and greater than 6 μm to map the distribution pattern of eolian dust in the marine sediment record of the Arabian Sea. The observed northwest-to-southeast gradient in eolian dust content indicates that eolian dust is supplied mainly by the northwesterly winds. The extent of the eolian dust distribution pattern over the ocean was used to approximate the position of the front (intertropical convergence zone) between the northwesterly winds and the southwest monsoon. A southward shift of this front during the last glaciation is indicated by changes in grain size and mineralogy (Sirocko and Lange, 1991; Sirocko et al., 1991, 1993).

The median grain size and the mass accumulation rate (MAR) of the terrigenous fraction in two sediment cores (RC27-61, ODP722; for location see Figure 1) retrieved from the Owen Ridge were used as paleoclimatic indicators of southwest monsoon wind strength and source area aridity by Clemens and Prell (1990, 1991), Clemens et al. (1991), and Murray and Prell (1991). Variations in lithogenic MAR appear to be associated with glacial-interglacial cycles, with highest fluxes recorded during glacial periods indicating increased source area aridity. The lithogenic grain-size record, exhibiting higher frequency variability (23 k.y.), has no strong relationship to glacial-interglacial cycles. This lack of relationship suggests that the climate change associated with variability in global ice volume is not a primary factor in determining the strength and timing of the southwest monsoon winds. Krissek and Clemens (1991) analyzed the bulk mineralogy of the terrigenous fraction of sediments from ODP722 on the Owen Ridge and concluded that temporal variations in mineralogical composition reflected climate-induced variations in weathering conditions during the late Quaternary.

Fluvial records.—

In the shelf and slope area near the Indus Delta, three canyon complexes have been recognized on seismics. They merge landward into one extensive erosional zone called the Indus Trough. The canyon complexes served as conduits for sediments supplied by the Indus River. Several large channel-levee systems radiate from each canyon complex, forming a channel-levee complex. The youngest complex comprises the recently active Indus Canyon (McHargue and Webb, 1986; Kolla and Coumes, 1987; Droz and Bellaiche, 1991). The two youngest large channel-levee systems of this complex have been mapped in detail by long-range side-scan sonar (GLORIA) (Kenyon et al., 1995). The study of Kenyon et al. (1995) resulted in a new scheme for labeling the Indus Fan channels on the basis of their relative ages. Von Rad and Tahir (1997) presented a detailed survey, including high-resolution seismic data and sediment cores, of the outer shelf and slope off the Indus Delta, including the Indus Canyon.

Changes in sea level are thought to be the dominant factor controlling turbidite deposition on large deep-sea fan systems. In addition, such process response is proposed for the Indus Fan (McHargue and Webb, 1986; Kolla and Coumes, 1987; Kolla and Macurda, 1988; McHargue, 1991; Kenyon et al., 1995; Prins and Postma, 1997; Von Rad and Tahir, 1997). Von Rad and Tahir (1997) indicated that due to the last glacial sea level lowstand, the Indus Canyon experienced maximum erosion and funneled turbidity currents to the Indus Fan. Accordingly, Prins and Postma (1997) concluded that the fall in sea level at approximately 25 ^{14}C k.y. initiated major lobe switching on the middle Indus Fan. The rise of sea level during the last deglaciation (~11.5 ^{14}C k.y.) cut off the Indus River as the main source of sediment for the middle fan.

Interplay of eolian and fluvial sources.—

The above observations indicate that the Arabian Sea sediments are mixtures of eolian dust and fluvial sediment, with the relative contributions of the two types of sediment depending on the location in the basin. At any given location, the relative contributions of materials from both sources are likely to have varied through time as well. Changes in continental aridity resulted in marked changes in the flux of eolian dust transported over the Arabian Sea. Changes in intensity and direction of the southwest monsoon, inferred from the eolian dust records of the western Arabian Sea, must have influenced the pattern of precipitation over the landmasses bordering the Arabian Sea to the west (Arabian Peninsula), the north (Pakistan), and the east (India). Changes in precipitation within the drainage basins of Indian-Pakistan rivers are expected to have controlled the water discharge and the suspended-sediment load of these rivers in the past

as well; however, possible late Quaternary changes in continental runoff and associated fluvial suspended-sediment supply to the Arabian Sea are sparsely documented. A suitable place to investigate changes in continental runoff and eolian dust supply by the northeast monsoon is the continental margin of Pakistan. Results obtained by detailed analysis of sediment cores from the western, central, and northern part of the Arabian Sea are presented in this study.

MATERIAL AND METHODS

Data Acquisition

Sediment cores used in this study were collected during the Netherlands Indian Ocean Programme (NIOP) on RV Tyro (Van der Linden and Van der Weijden, 1994), and during the SO90 PAKOMIN Expedition on RV Sonne (Von Rad et al., 1995). The cores, containing predominantly pelagic and hemipelagic sediments, were obtained from the Oman continental margin (cores NIOP484, 497), the Owen Ridge (core NIOP492), the Pakistan continental slope between the Murray Ridge and the Indus Canyon (cores NIOP451, 452, 455, and 458) along a slope-perpendicular transect, the eastern levee of the major channel radiating from the Indus Canyon (core SO90-169KL), and the levee of a small channel belonging to a large channel-levee system (system B, according to Kenyon et al., 1995) on the middle Indus Fan (core NIOP489). Figure 1 and Table 1 provide detailed information on the core locations.

Unsplit 1 m sections of cores NIOP458 and NIOP492 were logged at 1–2 cm intervals with a Bartington Instruments MS2 pass-through loop sensor mounted on a GEOTEC automated multisensor core logger to measure the bulk magnetic susceptibility. Samples were taken from the split 1 m sections at approximately 5–10 cm intervals. Fixed-volume samples were taken with a syringe, dried, and weighted for measurement of dry-bulk density (g/cm^3). One set of subsamples was washed and sieved to collect the fauna; another set of dried subsamples was used for analysis of the elemental chemical composition of the sediment (ICP). Wet subsamples were used for analysis of the grain size. The total carbonate content (biogenic and detrital) was calculated from the total Ca concentration (obtained from ICP analyses), using a correction for clay-derived Ca, which works well for carbonate-rich sediments: $CaCO_3 = 2.5[Ca_{tot} - (Ca/Al_{clay} \times Al_{tot})]$, where Ca/Al_{clay} is 0.345 (Turekian and Wedepohl, 1961; Shimmield et al., 1990).

Prior to the grain-size analysis, carbonate and organic carbon (only in sediments rich in organic carbon) were removed from the sediment samples by treatment with excess HCl and H_2O_2. Total dispersion of the sample was ensured by using a sonic dismembrator attached to the tank containing the suspended sample. The grain-size distribution of the siliciclastic fraction of 1102 samples was measured on a Malvern 2600 laser-diffraction size analyzer using a lens with 100 mm focal length. This configuration provided measurements in 32 discrete size classes between 0.5 and 188 μm (equivalent volume diameter) (see Table 2). The three coarsest size classes contain on average a small proportion of the total mass. They were amalgamated into a single class to reduce the number of variables to 30.

The $\delta^{18}O$ curves of NIOP458 and NIOP492 are based on the analyses of 20 handpicked specimens of the planktonic foraminifer *Neogloboquadrina dutertrei* (150–595 μm sieve fraction) per sample. The oxygen-isotopic composition of the carbonate shells was measured on a mass spectrometer. Age models have been constructed for cores NIOP458 and NIOP492 based on the correlation of the $\delta^{18}O$ records with the $\delta^{18}O$ record of core NIOP464 from the Murray Ridge (Figure 1). The age model of core NIOP464 was taken from Reichart et al. (1997). Linear sedimentation rates (LSR) (in cm/k.y.) were assumed between the age calibration points. Total mass accumulation rates (MAR) (total MAR = LSR × DBD; MAR in g/cm^2/k.y.) were calculated using the dry-bulk density (DBD) (in g/cm^3) of the sediment. Fractionated MARs (i.e., carbonate MAR and noncarbonate (siliciclastic) MAR) were determined by multiplying the total MAR with the carbonate fraction and with the siliciclastic fraction (1 – carbonate fraction).

TABLE 1. SEDIMENT CORES USED IN THIS STUDY

Core Number	Position (Lat. N, Long. E)	Area	Water Depth (m)	Core Length (m)	Number of Samples
NIOP451	23°40'.5, 66°03'.0	Upper Pakistan continental slope	542	17.06	163
NIOP452	22°56'.9, 65°28'.4	Lower Pakistan continental slope	1992	12.96	91
NIOP455	23°33'.4, 65°57'.0	Middle Pakistan continental slope	1002	14.50	117
NIOP458	21°59'.4, 63°48'.7	Upper Indus Fan	3001	16.31	163
SO90-169KL	22°38'.5, 66°49'.3	Channel levee, Indus Canyon	1283	11.65	114
NIOP489	17°56'.0, 65°52'.5	Channel levee, middle Indus Fan	3375	10.24	85
NIOP484	19°29'.8, 58°25'.7	Upper Oman continental slope	516	5.06+0.61	75
NIOP492	16°19'.0, 59°43'.6	Owen Ridge	2400	9.40	189
NIOP497	17°27'.0, 57°57'.6	Middle Oman continental slope	1885	8.83	105

End-Member Modeling

Linear mixing model.—

Linear mixing models of compositional data have been developed in various branches of the earth sciences (e.g., geochemistry, petrology, mineralogy, sedimentology) for the purpose of summarizing variation among a series of observations in terms of proportional contributions of (theoretical) end members (Jöreskog et al., 1976; Klovan and Miesch, 1976; Full et al., 1981, 1982; Renner, 1993, 1995; Weltje, 1994, 1997a). Compositional variation among a series of genetically related geological specimens (e.g., rock samples)

TABLE 2. SIZE RANGE FOR MALVERN LASER-DIFFRACTION SIZE ANALYZER*

Size Class	Lower Boundary (μm)	Upper Boundary (μm)	Size Class	Lower Boundary (μm)	Upper Boundary (μm)
1**	0.50	1.93	17	17.67	20.50
2	1.93	2.23	18	20.50	23.83
3	2.23	2.60	19	23.83	27.50
4	2.60	3.02	20	27.50	32.00
5	3.02	3.48	21	32.00	37.00
6	3.48	4.05	22	37.00	43.00
7	4.05	4.68	23	43.00	49.83
8	4.68	5.43	24	49.83	57.67
9	5.43	6.30	25	57.67	66.83
10	6.30	7.30	26	66.83	77.50
11	7.30	8.47	27	77.50	89.83
12	8.47	9.82	28	89.83	104.17
13	9.82	11.37	29	104.17	120.67
14	11.37	13.18	30	120.67	140.00
15	13.18	15.28	31	140.00	162.17
16	15.28	17.67	32	162.17	188.00

*Size range indicated for configuration of lens with 100 mm focal length.
**First class indicates amount of particles between detection limit (0.5 μm) and analyzed range (1.93 to 188 μm).

often can be attributed to physical mixing or mathematically analogous processes, such as fractional crystallization or selective transport and deposition. Data sets that conform to a linear mixing model can be expressed as mixtures of a fixed number of end members. The end members represent a series of fixed compositions that can be regarded as distinct subpopulations within the data set being analyzed. The linear mixing model is formulated as follows.

Compositional data are generally cast into the form of an $(n \times p)$ matrix X, with n rows representing observations, and p columns representing variables. By definition, compositional variables are non-negative and sum to a constant c, usually 1, 100, or 10^6 (for measurements recorded as proportions, percentages, or parts per million, respectively):

$$\sum_{j=1}^{p} x_{ij} = c \tag{1}$$

where

$$x_{ij} \geq 0$$

If compositional variation among a series of measured specimens results from a physical mixing process, each row of the matrix of compositional data X is a non-negative linear combination of the q rows of B, a matrix of end-member compositions. The matrix M represents the proportional contributions of the end members to each observation. In matrix notation, this perfect mixing can be expressed as

$$X = MB \tag{2}$$

subject to the following non-negativity and constant-sum constraints:

$$\sum_{k=1}^{q} m_{ik} = 1 \tag{3}$$

where

$$m_{ik} \geq 0$$

$$\sum_{k=1}^{p} b_{kj} = c \tag{4}$$

where

$$b_{kj} \geq 0$$

Although this representation is acceptable from an algebraic point of view, it fails to account for the fact that perfect mixing cannot be demonstrated in practice due to sampling and measurement errors in X; therefore, it is more realistic to assume that the data matrix X is made up of a systematic part X', attributable to perfect mixing, and a matrix of error terms E, representing nonsystematic contributions to X:

$$X = X' + E \tag{5}$$

It is assumed that the errors are relatively small, and that X' closely resembles X. By definition, the rows of X', the estimated matrix of perfect mixtures, consist of non-negative linear combinations M of q end-member compositions B:

$$X' = MB \tag{6}$$

The range of each variable in X' cannot exceed that of the corresponding variable in the end members B, due to the non-negativity constraints on M. By definition, the rows of X' are also compositions:

$$\sum_{j=1}^{p} x'_{ij} = c \tag{7}$$

where

$$x'_{ij} \geq 0$$

and therefore

$$\sum_{j=1}^{p} e_{ij} = 0 \tag{8}$$

These considerations lead to the following mathematical formulation of the general mixing model:

$$X = MB + E \tag{9}$$

subject to the constraints previously listed.

In many cases where compositional variation is believed to have been produced by mixing, the parameters of the mixing process are unknown. Recasting the observed compositional variation into a linear mixing model in the absence of prior knowledge about the number and composition of end members requires a solution of the bilinear (or explicit) mixing problem. This problem may be solved in two stages.

Estimating the number of end members.—

In the first modeling stage, the mixing space is defined by partitioning the data into X' and E ("signal" and "noise," respectively) for each possible number of end members by means of numerical algorithms rooted in fundamental concepts of vector analysis and linear algebra. The dimensionality (shape) of the data in p space reflects q, the number of linearly independent end-member vectors needed to span the mixing space. This implies that the number of end members can be estimated before their compositions have been calculated. The requirement of linear independence limits the maximum number of end members in inverse models of a mixing process to p, the number of variables measured.

Estimates of X' for various numbers of linearly independent end members $(2 \leq q \leq p)$ are obtained from constrained weighted least-squares approximations to the singular value decomposition of X (see Weltje, 1994, 1997a). Because the true number of end members and the errors associated with X are unknown, q can only be estimated by a comparison of the constrained linear approximations X' for different values of q to the original data X. In general, the goodness-of-fit increases as the number of end members is increased. The principle of parsimony is a useful guideline to the choice of q in view of the main objective of unmixing; i.e., to "explain" the observed compositional variation with a minimum number of end members. When the "best" representation X' has been selected, the number of linearly independent end members q has been fixed.

Estimating the end-member compositions.—

The problem to be solved in the second modeling stage consists of expressing X', the matrix of perfect mixtures, as the product of two matrices M and B. This is a constrained bilinear minimization problem that may be solved by means of coordinate transformation. The bilinear unmixing solution is intrinsically nonunique. Commonly, an

exact solution does not exist, and the number of approximate solutions is infinite. In other cases, there may be an infinite number of exact solutions. An unique solution thus requires specification of additional constraints.

A practical strategy is to provide additional constraints based on formalization of the notion of geological reasonableness. In the absence of prior knowledge, such a rule would allow the reconstruction of the "optimal" set of end-member compositions from which the observed variation could have been generated. Weltje (1994, 1997a) proposed that the optimal solution of the bilinear mixing problem should be based on the tradeoff between two apparently contradictory, but equally desirable, requirements: a fully non-negative mixing proportions matrix M and a conservative estimate of the end-member matrix B. The latter is non-negative by definition, so that the optimal solution can be regarded as a compromise between mathematical and geological feasibility. In other words, the optimal solution of the bilinear mixing problem (for a given value of q) consists of a set of end members that encloses as many of the data points as tightly as possible.

The preferred strategy for solving the bilinear mixing problem is an iterative estimation procedure, which does not require that all of the non-negativity constraints are taken into account at the same time (Full et al., 1981, 1982; Renner, 1993, 1995; Weltje, 1994, 1997a). A commonly adopted approach is to provide an initial guess of the end-member compositions, based on the properties of X'. Robust initial end-member estimates for a given value of q may be defined with nonhierarchical cluster analysis (cf. Full et al., 1982; Davis, 1986). The compositions represented by the cluster centers are projected into the mixing space to provide a starting point for iterative procedures aimed at locating a set of optimal end members (Figure 2A).

The mixing proportions matrix, M, corresponding to a set of trial end members B is generated by means of coordinate transformation, after which discrepancies between an ideal M and the current M are evaluated to define improvements to M. The end-member matrix B corresponding to the improved M is then calculated and optionally adjusted to comply with the non-negativity constraints. This procedure is iterated until the constraints on an optimal M are satisfied (Figure 2B, C). The end-member modeling algorithm proposed by Weltje (1994, 1997a) is guaranteed to converge if compositional variation in the estimated data reflects mixing of q linearly independent end members, because each successive set of end members encloses those generated in the previous iteration cycle.

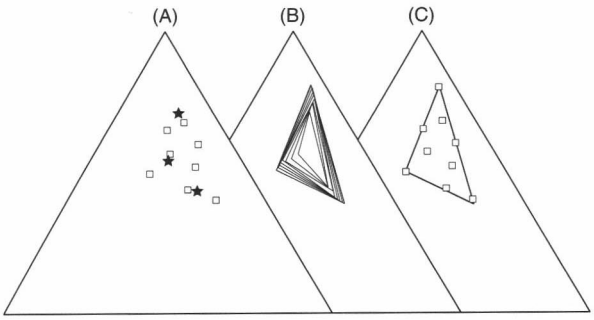

FIG. 2.—Illustration of the numerical end-member modeling algorithm. Construction of a ternary mixing model for a synthetic data set composed of three variables. Data set includes the true end members from which the mixtures were generated. (A) Initialization phase showing data points (squares) and cluster centers (stars). (B) A series of iterations (initial model and cycles 1–5, 7, 10, and 20 are shown). (C) Convergence is reached after 22 iterations. The modeled end members (vertices of the mixing space) closely approximate the true end members.

RESULTS

Goodness-of-Fit Statistics

A series of non-negative weighted least-squares approximations to the matrix of perfect mixtures X' was generated to estimate the number of end members. The minimum number of dimensions (end members) required for a satisfactory approximation of the data was estimated by calculating the coefficients of determination. The coefficients of determination represent the proportions of the variance of each variable (grain-size class) that can be reproduced by the approximated data. This proportion is equal to the squared correlation coefficient (r^2) of the input variables and their approximated values.

Figure 3A illustrates the distribution of the coefficients of determination across the grain-size classes for different values of q. Two size ranges are poorly reproduced by a two-end-member model: classes 13–20 and 27–30. The coefficients of determination for classes 27–30 are not weighted heavily in choosing the preferred end-member model because the mass in the coarse tails of the grain-size distributions comprises only a small fraction of the total mass in the data set. Reproducibility of the other grain-size range (classes 13–20) by the mixing model is considered to be of much greater importance, because this size range contains a considerable proportion of the total sediment mass. All of the 30 variables except size class 28 are adequately reproduced by a three-end-member

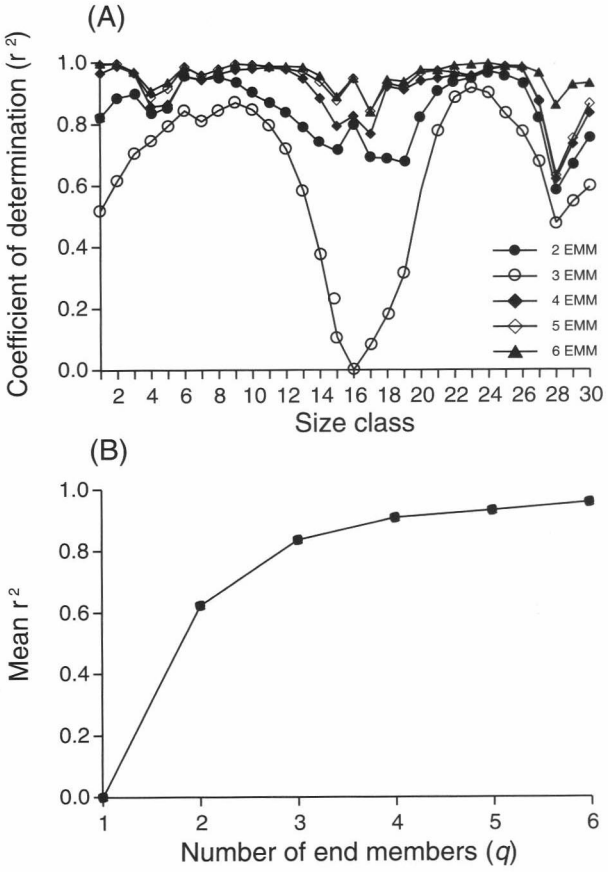

FIG. 3.—Goodness-of-fit statistics used to estimate the number of end members (see text for discussion). (A) Coefficients of determination for each size class. (B) Mean coefficient of determination across size classes. At least three end members are needed to reproduce all variables adequately; a two-end-member model shows distinct lack of fit in several size ranges. Use of four or more end members hardly improves the goodness-of-fit relative to a three-end-member model.

model, as indicated by their coefficients of determination that exceed 0.6 (equivalent to a correlation coefficient of 0.77).

The mean coefficient of determination across the grain-size classes (Figure 3B) increases when the number of end members is increased. The mean coefficient of determination for a three-end-member model is 0.83; i.e., on average, 83% of the variance in each grain-size class can be reproduced. A four-end-member model reproduces on average 90% of the input variances. The mean coefficient of determination increases only slightly for models with more than four end members. In conclusion, the goodness-of-fit statistics suggest that a three- or four-end-member model provides a reasonable choice in view of the contradictory requirements of parsimony on the one hand (i.e., a minimal number of end members) and reproducibility on the other hand.

Grain-size Distributions of End Members

Three- and four-end-member solutions were constructed to provide more insight into the nature of compositional variation in the data. The modeled end-member grain-size distributions for both models are shown in Figure 4, and the data are given in Table 3. A conspicuous result of the unmixing procedure is that all end members have a clearly defined dominant mode, whereas none are truly unimodal or of simple analytical form. This shows that the covariance structure of the data allows the extraction of subpopulations with fairly "natural" and "sensible" grain-size distributions; however, none of the parametric approaches discussed would have been capable of resolving such end members.

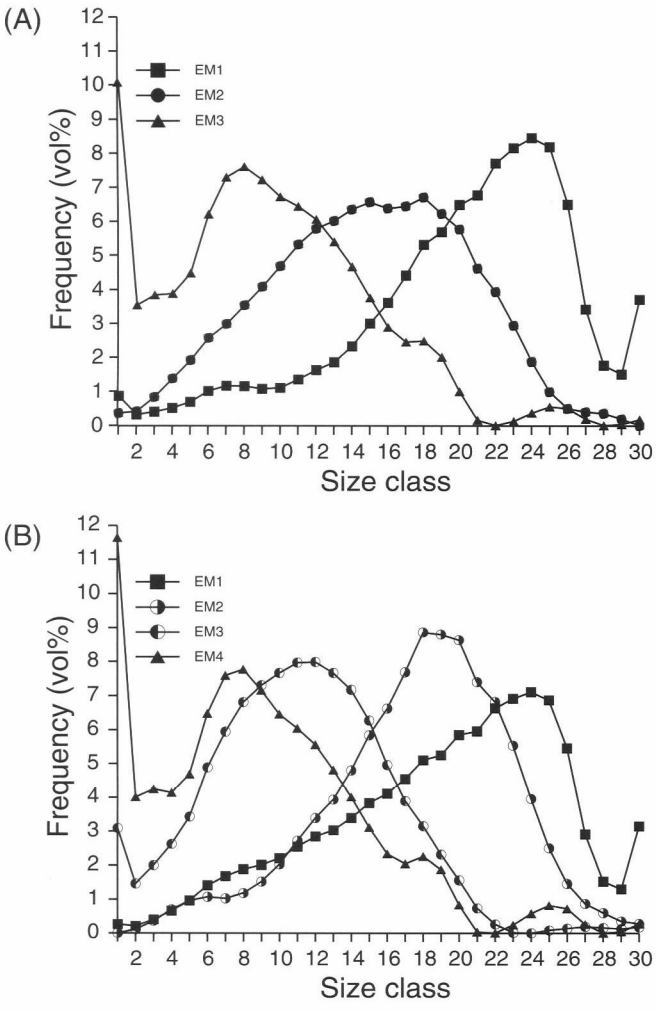

FIG. 4.—Modeled end members of Arabian Sea pelagic and hemipelagic siliciclastic sediments (see also Table 3). (A) Three-end-member model. (B) Four-end-member model.

TABLE 3. MODELED END MEMBERS OF ARABIAN SEA PELAGIC AND HEMIPELAGIC SILICICLASTIC SEDIMENTS

Three-End-Member Model				Four-End-Member Model				
Size Class	EM1 (%)	EM2 (%)	EM3 (%)	Size Class	EM1 (%)	EM2 (%)	EM3 (%)	EM4 (%)
1	0.86	0.36	10.07	1	0.26	0.00	3.09	11.64
2	0.32	0.41	3.54	2	0.21	0.11	1.46	4.01
3	0.40	0.83	3.84	3	0.40	0.36	2.00	4.25
4	0.51	1.38	3.88	4	0.66	0.70	2.62	4.14
5	0.69	1.92	4.48	5	0.96	0.96	3.43	4.69
6	1.01	2.57	6.21	6	1.41	1.07	4.89	6.48
7	1.16	2.98	7.30	7	1.68	1.02	5.94	7.59
8	1.15	3.54	7.61	8	1.88	1.18	6.81	7.77
9	1.07	4.09	7.22	9	2.01	1.52	7.30	7.16
10	1.10	4.68	6.72	10	2.20	2.03	7.66	6.46
11	1.35	5.31	6.44	11	2.54	2.72	7.96	6.04
12	1.63	5.78	6.06	12	2.84	3.39	7.98	5.56
13	1.86	6.01	5.39	13	3.03	3.94	7.66	4.81
14	2.32	6.35	4.66	14	3.39	4.80	7.17	4.01
15	2.99	6.56	3.75	15	3.83	5.84	6.27	3.11
16	3.61	6.38	2.88	16	4.11	6.62	4.96	2.33
17	4.41	6.44	2.44	17	4.55	7.68	3.89	2.04
18	5.30	6.70	2.47	18	5.10	8.86	3.15	2.25
19	5.68	6.22	2.00	19	5.25	8.80	2.31	1.87
20	6.48	5.76	0.99	20	5.85	8.63	1.56	0.83
21	6.76	4.61	0.15	21	5.95	7.40	0.74	0.03
22	7.70	3.93	0.00	22	6.63	6.82	0.26	0.00
23	8.15	2.93	0.12	23	6.91	5.54	0.01	0.24
24	8.45	1.87	0.36	24	7.11	3.96	0.00	0.58
25	8.18	0.98	0.54	25	6.87	2.50	0.08	0.82
26	6.49	0.49	0.49	26	5.46	1.46	0.14	0.72
27	3.41	0.39	0.18	27	2.91	0.87	0.19	0.26
28	1.76	0.35	0.00	28	1.53	0.60	0.16	0.00
29	1.50	0.18	0.03	29	1.30	0.35	0.13	0.04
30+	3.70	0.00	0.17	30+	3.15	0.28	0.18	0.27

The first end members (EM1) of both models have a modal grain size of approximately 50 μm (class 24). End member 3 (EM3) of the three-end-member model is almost identical to end member 4 (EM4) of the four-end-member model. Both have a modal grain size of approximately 5 μm (class 8). End member 2 (EM2) of the three-end-member model has a bimodal grain-size distribution with modes around 14 and 22 μm (classes 15 and 18). End members 2 and 3 (EM2 and EM3) of the four-end-member model have modes at 22 and 9 μm (classes 12 and 18), respectively.

The fact that both models are about equally good in approximating the observed variation in the data set is partly a consequence of the similarity of their coarsest and finest end members. The lack of improvement in goodness-of-fit is further clarified by expressing the end members of the three-end-member model as mixtures of the end members of the four-end-member model (Figure 5A). The least-squares mixing coefficients are shown in Figure 5B. For instance, EM2 of the three-end-member model is closely approximated by a mixture of 58% EM2 and 42% EM3 of the four-end-member model. In the four-end-member model, the EM2:EM3 ratio varies on average only slightly about this mean value. Consequently, the marginal improvement of the goodness-of-fit reflects the addition of end members that explain only a small fraction of the compositional variation in the data. Because there are no reasons to prefer the four-end-member model, we investigate the applicability of the three-end-member model.

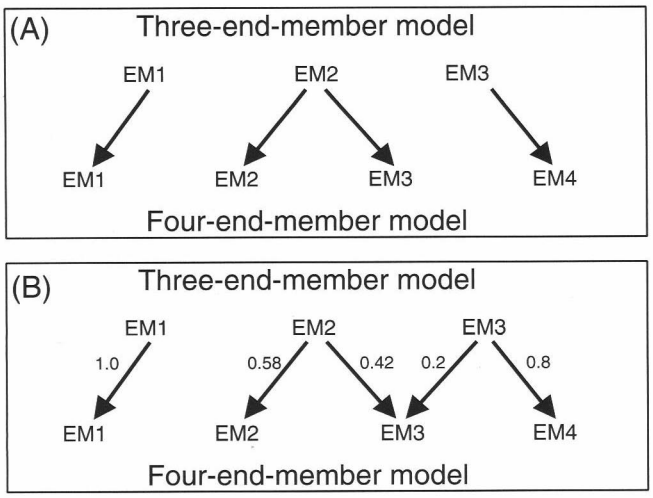

FIG. 5.—(A) Most likely combinations of the end members of the three- and four-end-member models. (B) Least-squares mixture coefficients.

Three-End-Member Model

Comparison between observed and modeled grain-size distributions.—

In the ternary mixing model, spatial and temporal changes in grain-size distributions are expressed as changes in the relative abundances of the end members. In spite of the significant size reduction of the data set (compressing 30 size classes into three mixing coefficients), the complete grain-size distribution can still be reconstructed, in contrast with a "traditional" description in terms of three graphic or moment measures. The goodness-of-fit of each modeled grain-size distribution can be visualized by comparing it to the observed grain-size distribution. Figure 6 shows the modeling results of two samples from core NIOP492. Sample NIOP492/35 (Figure 6A) is composed of EM2 (66%) and EM3 (34%), whereas sample NIOP492/110 (Figure 6B) is a mixture of all three end members (23% EM1, 57% EM2, 20% EM3).

Grain-size-spectra diagrams (cf. Dowling, 1977) of the observed and modeled records of core NIOP492 are shown in Figure 7A and *B*. These diagrams are contour maps of the mass proportions per size class in the space-size domain. In this particular example, "space" refers to the sample numbers plotted in stratigraphic order (sample 1 is top and sample 189 is base of core NIOP492). The size domain has been subdivided into equal size intervals on a logarithmetic scale [widths 0.2 ϕ; units of mass are expressed as volume percentages (vol.%) per size interval].

The modeled grain-size-spectra diagram (Figure 7B) is somewhat less irregular than the observed grain-size-spectra diagram (Figure 7A). This reflects the reduction of the variance, which has simplified the grain-size distributions and (provided that the basic assumptions are valid and the model parameters have been successfully estimated) suppressed the noise in the observations. The overall pattern observed in the space-size domain can be fairly well reproduced with three end members. Figure 7C shows the "residuals" in the space-size domain; i.e., the difference between the observed and modeled grain-size distributions in terms of absolute deviations (vol.% per size interval). The summed absolute deviations for each observation (Figure 7D) are of the same order of magnitude as typical sampling and measurement errors for the studied core material, which have been determined from replicate analyses. We conclude that the three-end-member model successfully reproduces the compositional variation in the data.

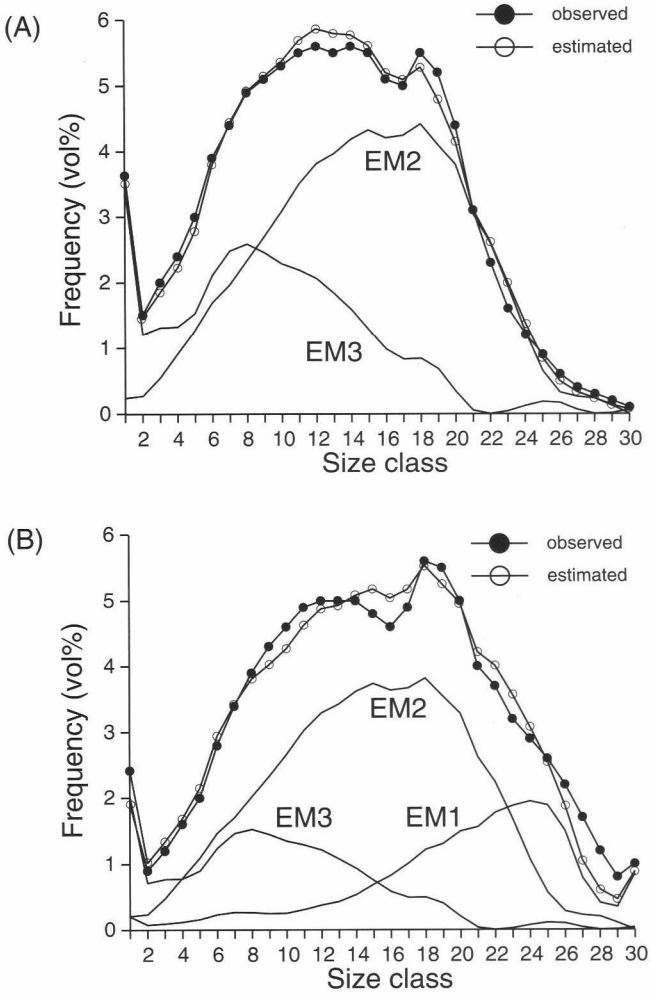

FIG. 6.—Approximation of observed grain-size distributions by the three-end-member model. (A) Estimated composition of sample NIOP492/35: 0% EM1, 66% EM2, and 34% EM3. (B) Estimated composition of sample NIOP492/110: 23% EM1, 57% EM2, and 20% EM3.

Spatial variations in mixing coefficients.—

The total range of compositional variation has been visualized in a ternary diagram (Figure 8) of which the modeled end members form the three vertices (hypothetical observations A, C, E). Three hypothetical binary mixtures are shown as observations *B*, D, F, and a ternary mixture as observation G. The individual data points of the estimated compositions of the 1102 samples form a large scatter in the ternary mixing space (Figure 9A). Binary mixtures of EM1 and EM3 (cf. hypothetical observation F in Figure 8) are practically absent. When the data of the cores from the two geographical regions, the western and the northern Arabian Sea, are plotted separately in ternary diagrams, some clear trends become visible.

Samples from cores NIOP484, 492, and 497 can be described as mixtures of predominantly EM1 and EM2 because they plot on the left side of the ternary diagram (Figure 9B). The sediments in the cores from the northern Arabian Sea (NIOP451, 452, 455, 458, and SO90-169KL) can be described as mixtures of predominantly EM2 and EM3 (Figure 9C). The same applies to core NIOP489 from the central part of the Arabian Sea.

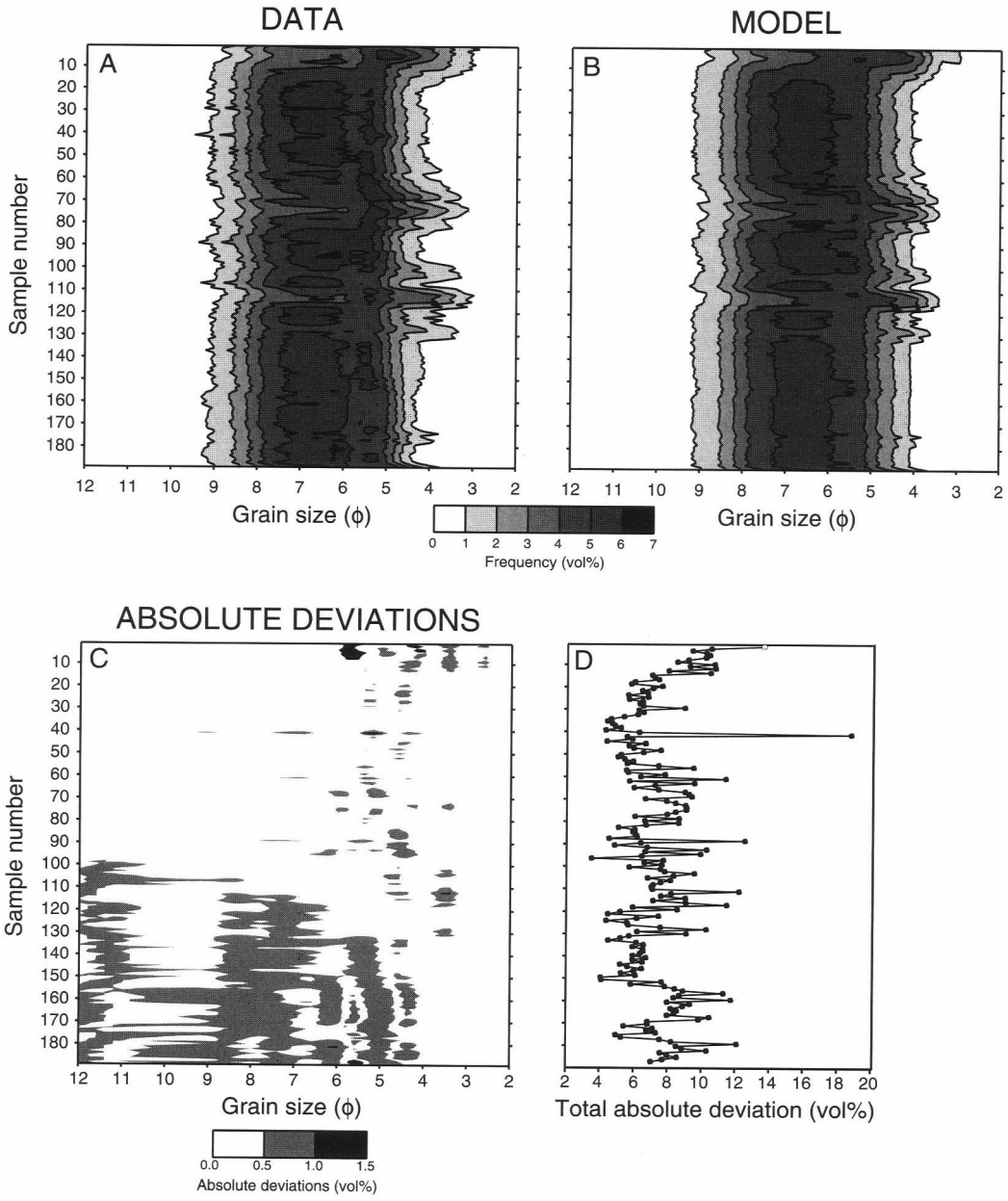

FIG. 7.—Modeling results of core NIOP492. (A) Grain-size-spectra diagram of observed grain size distributions (vol.% per 0.2ϕ interval). (B) Estimated grain-size distributions according to the three-end-member model. Note smoothing effect due to reduced variance of the mixing model. (C) Contour map of absolute deviations between data and model. (D) Summed total absolute deviation per sample.

Spatial changes in average sediment composition have been visualized by plotting the 90-95-99% confidence regions of the population means of the sediments sampled in each core (using an algorithm described by Weltje, 1997b). Figure 10A shows the confidence regions associated with cores from the western Arabian Sea, and Figure 10B shows those from the northern and central parts of the Arabian Sea. The grain-size population means at the sites of cores NIOP484, 492, and 497 differ significantly from one another at a 99% confidence level because they do not overlap one another (Figure 10A). In the transect NIOP 484-497-492 (west to east, shallow to deep, proximal to distal; Figure 1), the average composition changes from EM1-dominated sediments toward EM2-dominated sediments.

The population means of the grain-size distributions at core sites in the northern and central Arabian Sea differ significantly from one another at a 99% confidence level, except those of cores NIOP452 and NIOP455, which differ significantly from one another at a 90% confidence level (Figure 10B). In the transect NIOP451-455-452-458 (north to south, shallow to deep, proximal to distal; Figure 1) the ratio EM2:EM3 gradually decreases, reflecting a spatial trend in the composition of the sediments. Sediments from core SO90-169KL, obtained from the levee south of the Indus Canyon, have relatively low EM2:EM3 ratios and low EM1 content compared with NIOP455, which was obtained from the same water depth. The sediments especially from core NIOP489 have high proportions of EM3. In this core, samples are mixtures of EM2 and EM3 exclusively.

Interpretation of end members.—

End members of a series of grain-size distributions may be related to two kinds of processes (Syvitski, 1991). When two end-member grain-size distributions are mixed in various proportions, they provide a suite of sediment samples with attributes falling between these end members. Such sediments could represent true mixtures of materials,

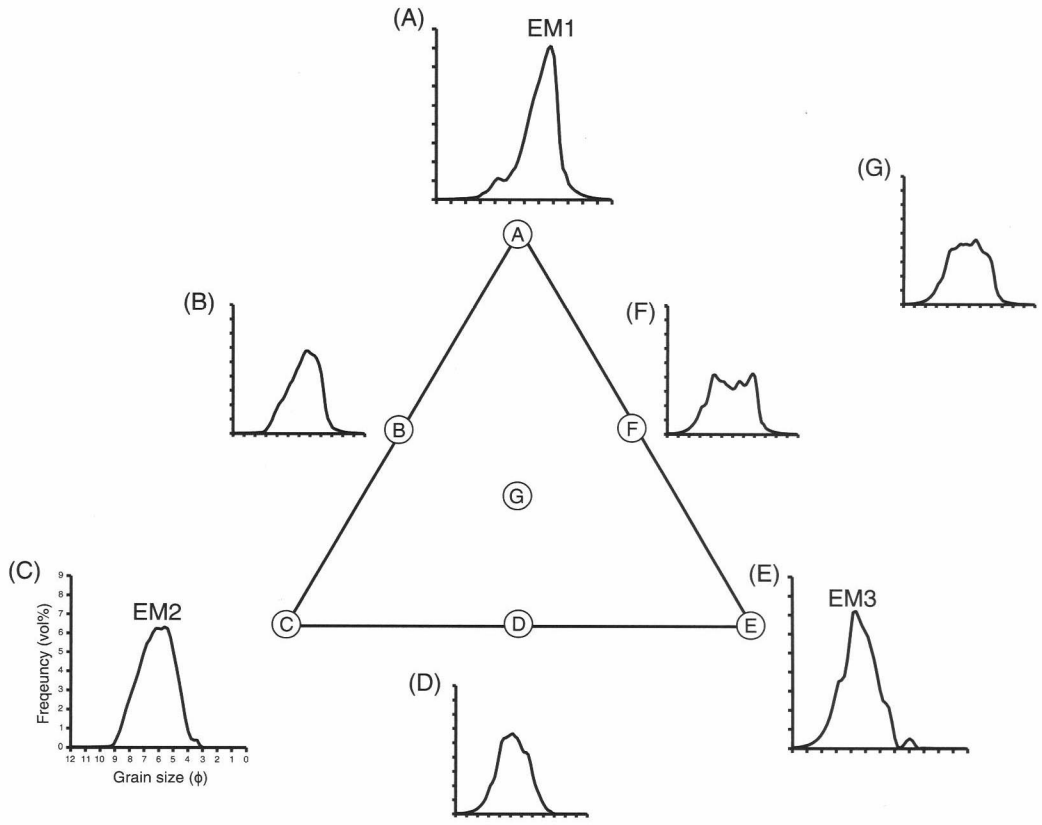

FIG. 8.—Three-end-member model plotted in ternary diagram showing grain-size distributions of end members (A, C, E) and hypothetical mixtures (B, D, F, G).

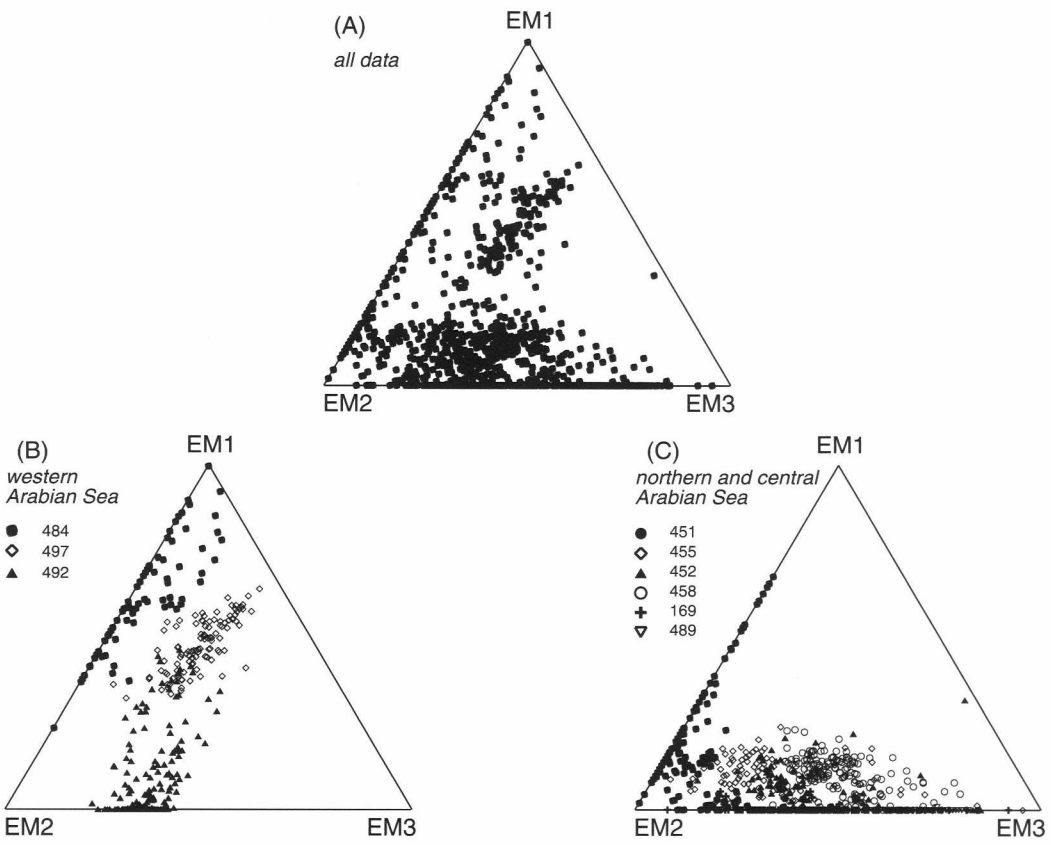

Fig. 9.—(A) Mixing model of the 1102 Arabian Sea sediment samples. (B) Binary mixing of end members EM1 and EM2 prevails in the western Arabian Sea sediments (NIOP484, 492, and 497). (C) Binary mixing of end members EM2 and EM3 prevails in the northern and central Arabian Sea sediments (NIOP451, 452, 455, 458, 489, and SO90-169KL).

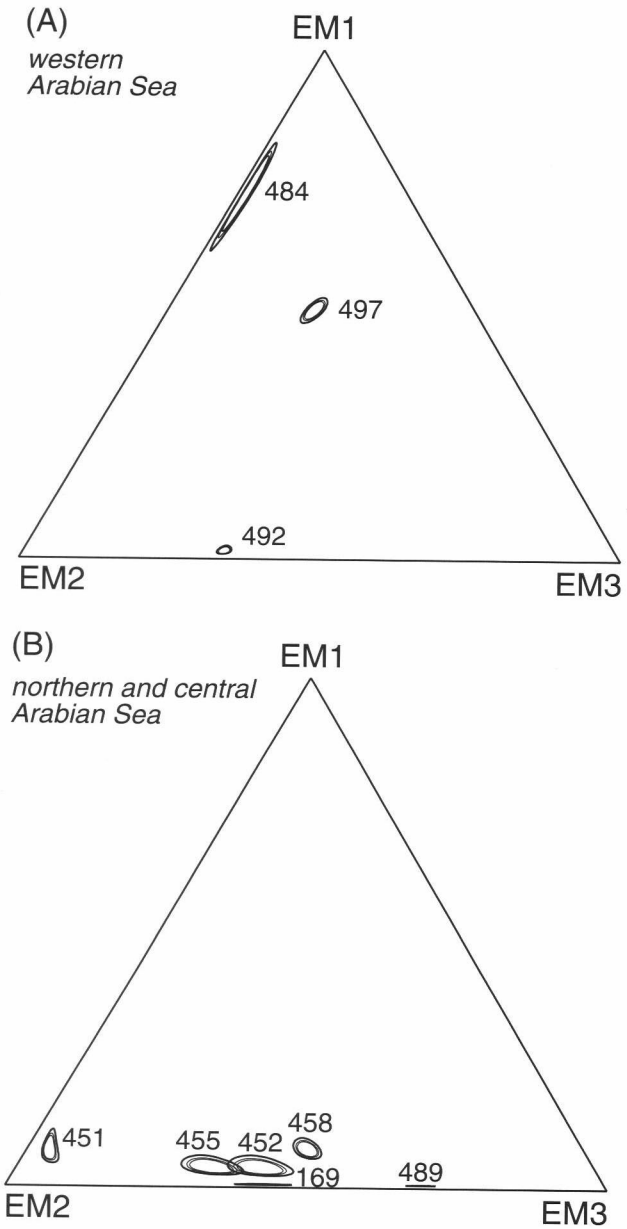

FIG. 10.—Confidence regions (90-95-99%) of the population means of cored sediments in ternary mixing space. (A) Population means of sediments from the western Arabian Sea (NIOP484, 492, and 497). (B) Population means of sediments from the northern and central Arabian Sea (NIOP451, 452, 455, 458, 489, and SO90-169KL).

which have been transported by independent mechanisms, supplied by different sources; however, end-member distributions also may represent the beginning and end of a selective process of transport and deposition. For instance, selective mechanisms operating during unidirectional transport and deposition produce sediments whose grain-size distributions change systematically with distance from the source. Unmixing of such data sets results in "proximal" and "distal" end members; hence, the number of actual sediment sources is per definition equal to or less than the number of end members.

Different spatial trends in sediment composition have been recognized in both the western and northern Arabian Sea. Along the western Arabian Sea transect the average composition changes basinward from EM1-dominated sediments to EM2-dominated sediments. Along the northern Arabian Sea transect, the average composition changes basinward from EM2-dominated sediments to EM3-dominated sediments. Both trends represent basinward fining.

The compositional trend along the western transect is illustrated by the grain-size distributions of four representative samples of approximately the same age (early Holocene, 10 k.y. BP) from cores NIOP484, 497, 492, and 489 (Figure 11). Analysis of the chemical composition and mineralogy of selected size ranges of these four samples (M. A. Prins, unpublished data) reveals a high degree of compositional similarity, which strongly suggests that the sediments were derived from the same source. The presence of the clay mineral palygorskite in each of the samples indicates that the dominant source of the terrigenous fraction is the Arabian peninsula (Kolla et al., 1976; Sirocko and Lange, 1991). The absence of large river systems debouching in the western Arabian Sea, coupled with the location of the cores (NIOP492 on the Owen Ridge and NIOP489 on the middle Indus Fan), allow us to exclude the possibility that the bulk of the sediment of Arabian provenance represents anything other than eolian dust (the NIOP489 sample of eolian origin was taken from a calcareous ooze unit that drapes the Pleistocene river-derived sediments of the Indus Fan). The basinward-fining trend is expressed as changes in the relative proportions of the end members. The ratio EM1:EM2 decreases, whereas the proportion of EM3 increases when going from the Oman continental margin toward the Indus Fan. The "proximal-distal" fining trend most likely represents the result of preferential settling of the coarse fraction during eolian transport from the desert source. EM1 may thus be interpreted as proximal, relatively coarse-grained eolian dust, and EM2 as distal, relatively fine-grained eolian dust. These end members thus represent the "beginning" and "end" of a depositional process (cf. Syvitski, 1991).

The Pleistocene channel-levee sediments of the middle Indus Fan (NIOP489) are dominated by contributions of EM3 muds that were deposited at high rates (30 g/cm²/k.y.). Mineralogy and chemical composition of the turbidite muds are identical to those of sediments obtained from the Indus Canyon, indicating that the dominant source of the terrigenous fraction is the Indus River (M. A. Prins, unpublished data). Turbidity currents supplied huge amounts of river-derived sediments through the Indus Canyon, which were eventually deposited on the middle Indus Fan within the main sediment depocenters (Kolla and Coumes, 1987; Kenyon et al., 1995). The finest fractions are deposited out of the low-density low-velocity "tails" of the turbidity currents within and well outside the main depocenters of the river-derived silts and sands. In view of the location of core NIOP489, we conclude that EM3 represents fluvial mud supplied by the Indus River and deposited out of low-density turbidity currents. The EM3 muds deposited on the continental slope and upper Indus Fan, west of the Indus Canyon, probably are derived from the Pakistan shelf area. These muds may have been supplied across the shelf directly by the Indus River, most likely during flooding or as wave-induced sediment resuspension clouds. Re-suspension of shelf muds is probably also the most likely process of dispersal of the EM3 muds in the western Arabian Sea where river input is insignificant.

In summary, sediments obtained from the western Arabian Sea are essentially mixtures of coarse- and fine-grained eolian dust (EM1 and EM2), whereas sediments from the northern Arabian Sea essentially are mixtures of fine-grained eolian dust and fluvial mud (EM2 and EM3). The presence of multiple grain-size trends in the same basin fill clearly indicates that temporal variations in

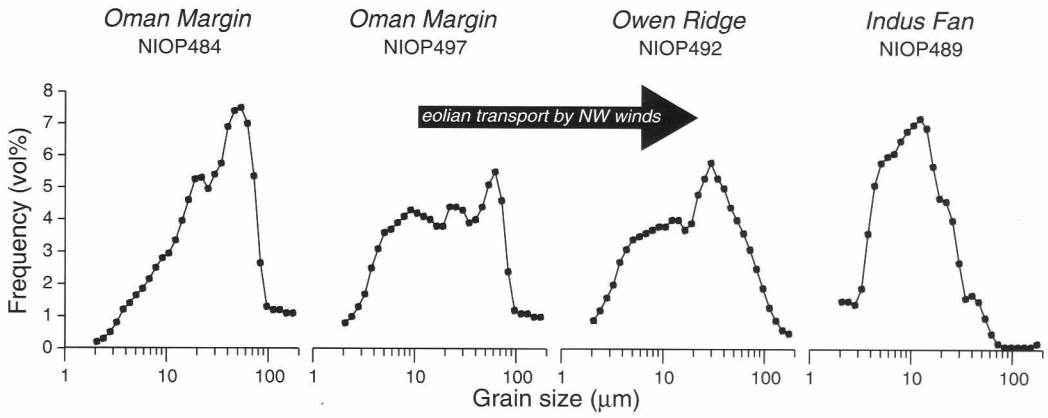

FIG. 11.—Grain-size distributions of four early Holocene eolian-dust–dominated samples obtained along a transect approximately perpendicular to the Arabian coast. Progressive fining of the sediment in a downwind direction is reflected in the relative proportions of the end members. Compositions of the samples expressed as EM1/EM2/EM3: NIOP484/60 79/21/0; NIOP497/4 53/20/27; NIOP492/4 46/34/20; NIOP489/117 0/59/41.

grain size must be interpreted with great care. The mixing structure of the Arabian Sea sediments suggests that paleoclimatic information may be extracted from the grain-size records as follows. The ratio EM1:EM2 indicates the grain size of the eolian dust, and therefore may be used as a proxy for changes in paleowind speed. The ratio (EM1 + EM2):EM3 indicates the relative importance of the mode of sediment transport during time of deposition; i.e., eolian transport vs. low-density turbidity transport. The input of eolian dust increases during periods with an arid continental climate, whereas the input of fluvial mud increases during periods with a humid continental climate. Consequently, changes in the ratio (EM1 + EM2):EM3 may be used as a proxy for changes in continental aridity.

Comparison of Records from the upper Indus Fan and Owen Ridge

Sediment flux.—

Temporal changes in the flux and composition of sediments from the western and northern Arabian Sea are illustrated for two sediment cores: NIOP458 from the upper Indus Fan and NIOP492 from the Owen Ridge. The *Neogloboquadrina dutertrei* $\delta^{18}O$ records of cores NIOP458 and NIOP492 were correlated with the $\delta^{18}O$ record of core NIOP464 to convert depth into age (Figure 12). This correlation shows that the sedimentary records in core NIOP492 and NIOP458 span the last 186 k.y. (isotopic stages 1–6) and 208 k.y. (isotopic stages 1–6, and part of isotopic stage 7).

The carbonate records of cores NIOP458 and NIOP492 show some marked differences. The carbonate content in core NIOP458 ranges between 9 and 50 wt.% (Figure 13A), whereas in core NIOP492 the carbonate content ranges between 45 and 75 wt.% (Figure 13B). The carbonate content on the Owen Ridge (NIOP492) tends to be highest during the interglacial stages (1, 3, 5). A good anticorrelation between magnetic susceptibility and carbonate content can be observed in core NIOP492, whereas in core NIOP458 this correlation is less clear.

In this study, the contribution of terrigenous material to the sediment was simply taken as total mass minus carbonate mass. This method underestimates the proportion of terrigenous material in the presence of detrital carbonate, and overestimates the proportion of terrigenous material in the presence of biogenic opal and organic carbon. Sirocko et al. (1991) showed that the contribution of detrital carbonates to the sediment close to the coast of Oman reaches maxima of greater than 10%, but rapidly decreases basinward. The average contribution of detrital carbonates to the sediment is estimated as less than 5% in the region where cores NIOP458 and NIOP492 were obtained. According to Murray and Prell (1991), opal and organic carbon are only minor components of the Owen Ridge sediments. Organic carbon content ranges from 0.4 to 2.0%.

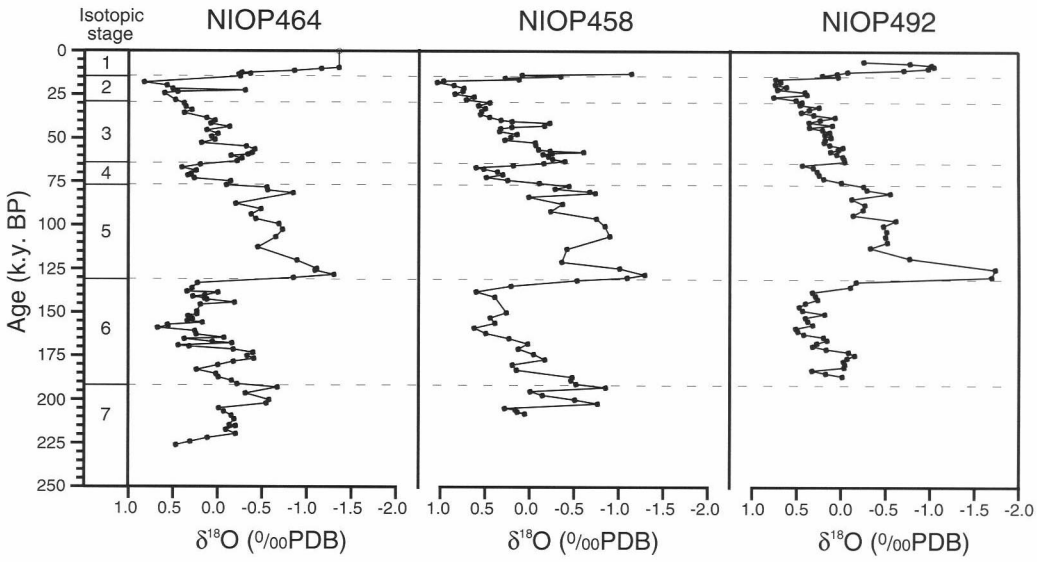

FIG. 12.—Age models of cores NIOP458 and NIOP492 based on correlation of the $\delta^{18}O$ (*N. dutertrei*) records with core NIOP464.

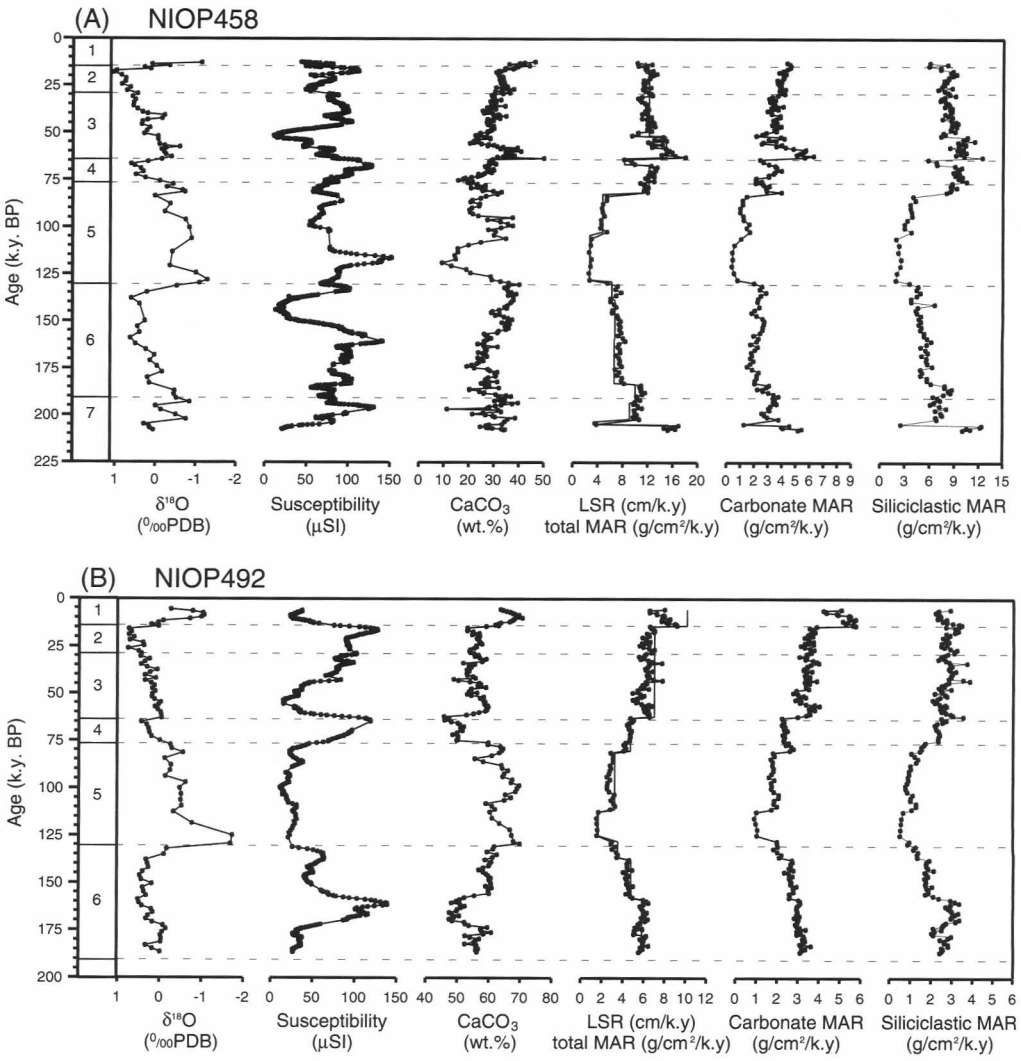

FIG. 13.—Time series of $\delta^{18}O$ (*N. dutertrei*), magnetic susceptibility, carbonate content, linear sedimentation rates (LSR) and mass-accumulation rates (MAR). (A) NIOP458, upper Indus Fan. (B) NIOP492, Owen Ridge.

Opal content ranges from 0.5 to 2.5%, with distinct maxima occurring in interglacials. SEM (scanning electron microscope) inspection of selected grain-size fractions of samples from NIOP492 showed that the bulk of the biogenic opal is confined to the sand fraction (>63 μm). In core NIOP458, the organic carbon content ranges between 0.2 and 2.3% (G. J. Reichart, 1997, personal communication), and SEM inspection shows that the opal content is insignificant. All of these observations indicate that our approximation of the terrigenous contribution is reasonably accurate.

Total linear sedimentation rates (LSR) (in cm/k.y.) and total mass accumulation rates (total MAR) (in g/cm²/k.y.) are highest during glacials at both sites. The same holds for the carbonate MAR and siliciclastic MAR. Although the carbonate MAR are about equal at both sites throughout the studied time period, the siliciclastic MAR is about three times higher at site NIOP458 when compared with the values recorded at site NIOP492. Hence, the carbonate content may be interpreted as a dilution signal (cf. Shimmield et al., 1990), rather than an indicator of dissolution or changes in surface productivity.

Median grain size.—

Time series of the median grain size of cores NIOP458 and NIOP492 are shown in Figure 14. In core NIOP458, an almost perfect positive correlation between the median grain size and the $\delta^{18}O$ records is observed, indicating relatively fine-grained mud deposition during interglacial stages (1, 3, 5, 7) and relatively coarse-grained mud deposition during glacial stages (2, 4, 6). Within stage 5, even the substages are expressed in the grain size record (substages 5.1, 5.3, and 5.5 are relatively fine grained). The opposite is observed in the record of core NIOP492, which shows an almost perfect negative correlation between the median grain size and the $\delta^{18}O$ curves. The glacials are characterized by deposition of relatively fine-grained muds, while during interglacials relatively coarse-grained muds are deposited. The changes in grain size during the substages of isotopic stage 5 are clearly visible.

Relative end-member contributions.—

In core NIOP458 (Figure 15A), the relative contributions of EM1 tend to be highest (up to 24%) during glacials and lowest (down to 0%) during interglacials. The relative contributions of EM2 show a similar pattern of relative contributions that vary between 17 and 65%. Consequently, the relative contributions of EM3 (26–78%) are highest during interglacials. The proportional contributions of EM1 to the sediment at site NIOP492 (Figure 15B) reach values up to 46% during interglacial stages 1, 3, and 5

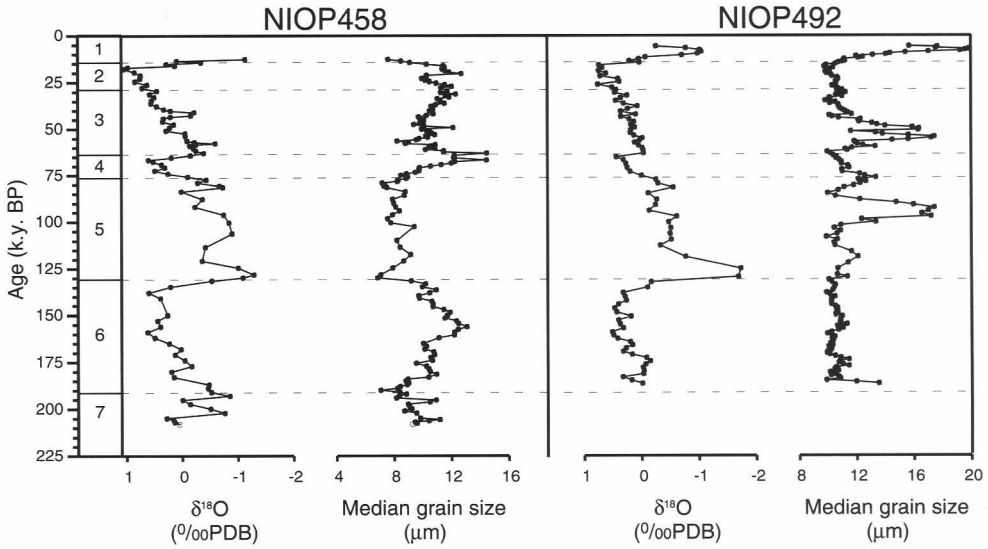

FIG. 14.—Variations in median siliciclastic grain size in cores NIOP458 and NIOP492 compared with climate change as indicated by the $\delta^{18}O$ (*N. dutertrei*) records.

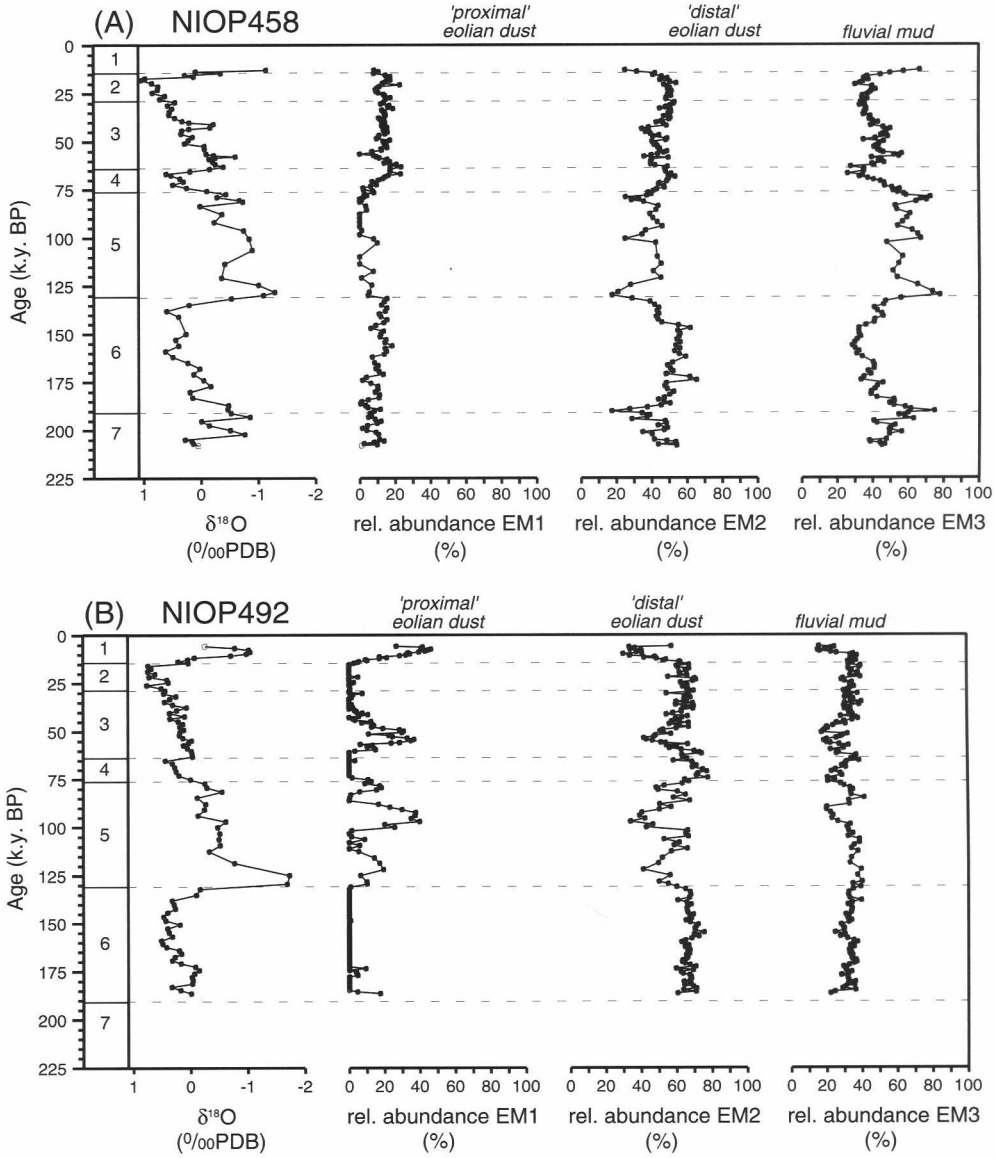

FIG. 15.—Variations in relative abundances of end members compared with climate change as indicated by the $\delta^{18}O$ (*N. dutertrei*) records. (A) Core NIOP458. (B) Core NIOP492.

(substages 5.1, 5.3, and 5.5). They are smallest during glacials and substages 5.2 and 5.4. The relative abundances of EM2 and EM3 in core NIOP492 are highest during glacials. Between 30 and 78% of the siliciclastic fraction of the sediment consists of EM2, while EM3 ranges between 15 and 41%.

A comparison of the coarse-grained eolian dust (EM1) records of the western and northern Arabian Sea reveals a negative correlation. The same applies to the fluvial mud (EM3) records of both areas; however, the fine-grained eolian dust (EM2) records show a strong positive correlation. The remarkable difference between the median-grain-size records of the two sites can now be fully explained in terms of different sediment supply mechanisms. Grain-size distributions on the upper Indus Fan (NIOP458) mainly reflect mixing of eolian dust and fluvial mud in varying proportions. At this locality, the median grain size may be used as a proxy for changes in continental aridity. Variations in median grain size on the Owen Ridge (NIOP492) are mainly controlled by the relative abundances of the two eolian dust end members. At this locality, the median grain size may be used as a proxy for paleowind strength (although the arithmetic mean is a much more sensitive measure for this particular purpose).

End-member ratios: proxies for continental aridity and wind strength.—

The use of the end-member ratios EM1:EM2 and (EM1 + EM2): EM3 as paleoclimate proxies is illustrated in Figure 16. Confidence regions of the population means of glacial (stages 2–4, 6) and interglacial (stages 1, 5, 7) sediments have been plotted separately for cores NIOP492 and NIOP458 in ternary diagrams. The subdivision into glacial and interglacial stages highlights the most important compositional variation in the terrigenous sediment records. In both cores, the interglacial population differs significantly from the glacial population at a 99% confidence level because these regions do not overlap one another.

Lines drawn from the EM3 vertex of the ternary diagram toward the opposite side of the diagram represent compositions with equal EM1:EM2 ratios. Likewise, compositions with equal (EM1 + EM2): EM3 ratios are located on lines parallel to the upper left edge of the diagram. Such lines have been drawn through the population means of the interglacial and glacial samples to illustrate the temporal differences of the ratios at both coring sites.

Changes in EM1:EM2 ratio between glacial and interglacials portray differences in paleowind speed over time, denoted by ΔWS in Figure 16. At site NIOP492, the highest EM1:EM2 ratios are recorded during interglacial periods. In contrast, at site NIOP458 the highest EM1:EM2 ratios are recorded during glacial periods. Differences in continental aridity between glacials and interglacials are shown as changes in (EM1 + EM2):EM3 ratio, denoted by ΔCA in Figure 16. High (EM1 + EM2):EM3 ratios are recorded during glacials stages at site NIOP458 indicating increased continental aridity during glacial times. At site NIOP492, the differences in the (EM1 + EM2):EM3 ratios between the glacial and interglacial periods are not significant.

An alternative indicator for paleowind speed may be obtained by calculating the grain-size distribution of eolian dust by subtracting the proportion of fluvial mud (EM3) from the observed grain-size distributions of the total terrigenous fraction. This approach circumvents possible discrepancies between data and model (Figure 7C) by operating directly on the raw data. The eolian dust grain-size record of core NIOP492 (Figure 17A) shows high-frequency variations with sharp peaks, indicating intensified wind speeds, during the interstadials and interglacial stages 1, 3, 5.1, 5.3, and 5.5. In contrast, within

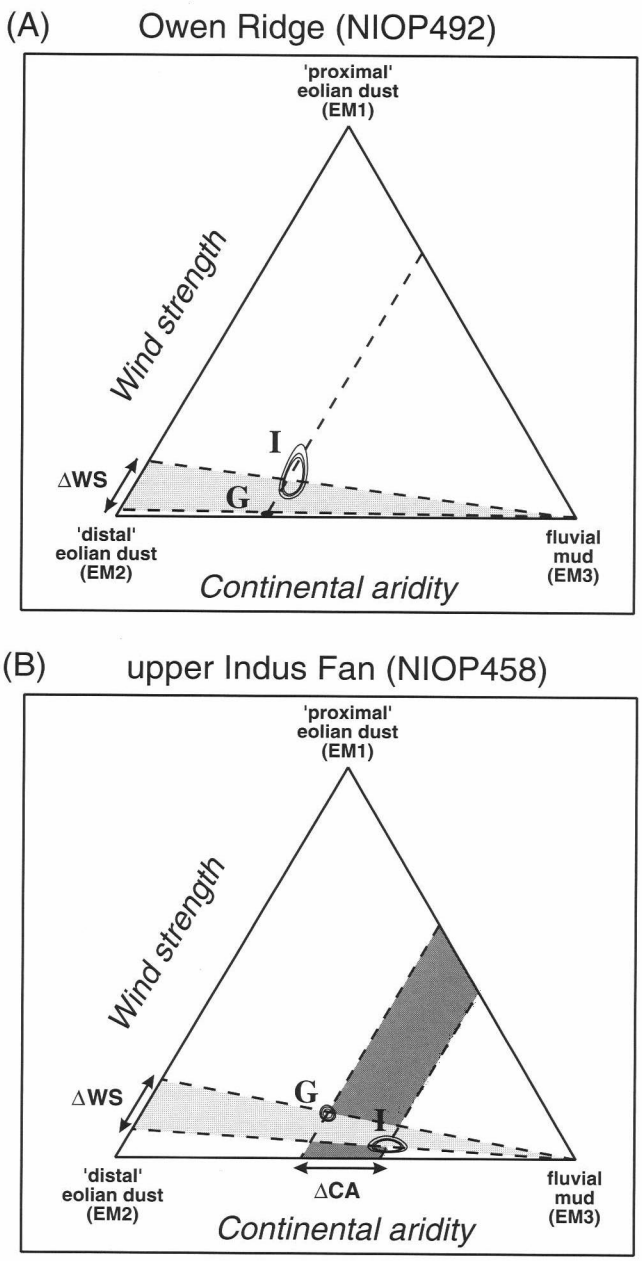

FIG. 16.—Ratios of end-member contributions as proxies for variation in wind strength (ΔWS) and continental aridity (ΔCA), illustrated by plotting the confidence regions (90-95-99%) of glacial (G) and interglacial (I) population means. (A) EM1:EM2 ratios in NIOP492 indicate stronger summer monsoons during interglacials. (B) EM1:EM2 ratios in NIOP458 indicate stronger winter monsoons during glacials. (EM1 + EM2):EM3 ratios in NIOP458 indicate increased continental aridity during glacials.

core NIOP458, small eolian dust grain sizes (Figure 17B) indicate weak dust-transporting winds during the interstadials and interglacial stages 1, 3, 5.1, 5.3, 5.5, and 7. The detailed NIOP458 record of the log-ratio (EM1 + EM2):EM3 is shown in Figure 17C. The observed high-frequency variation in this record, portraying variations in continental aridity on the Pakistan-Indian peninsula, correlates in detail with the variations observed in the $\delta^{18}O$ record of core NIOP458 (Figure 17D). Variations in continental aridity are associated with glacial-interglacial cycles.

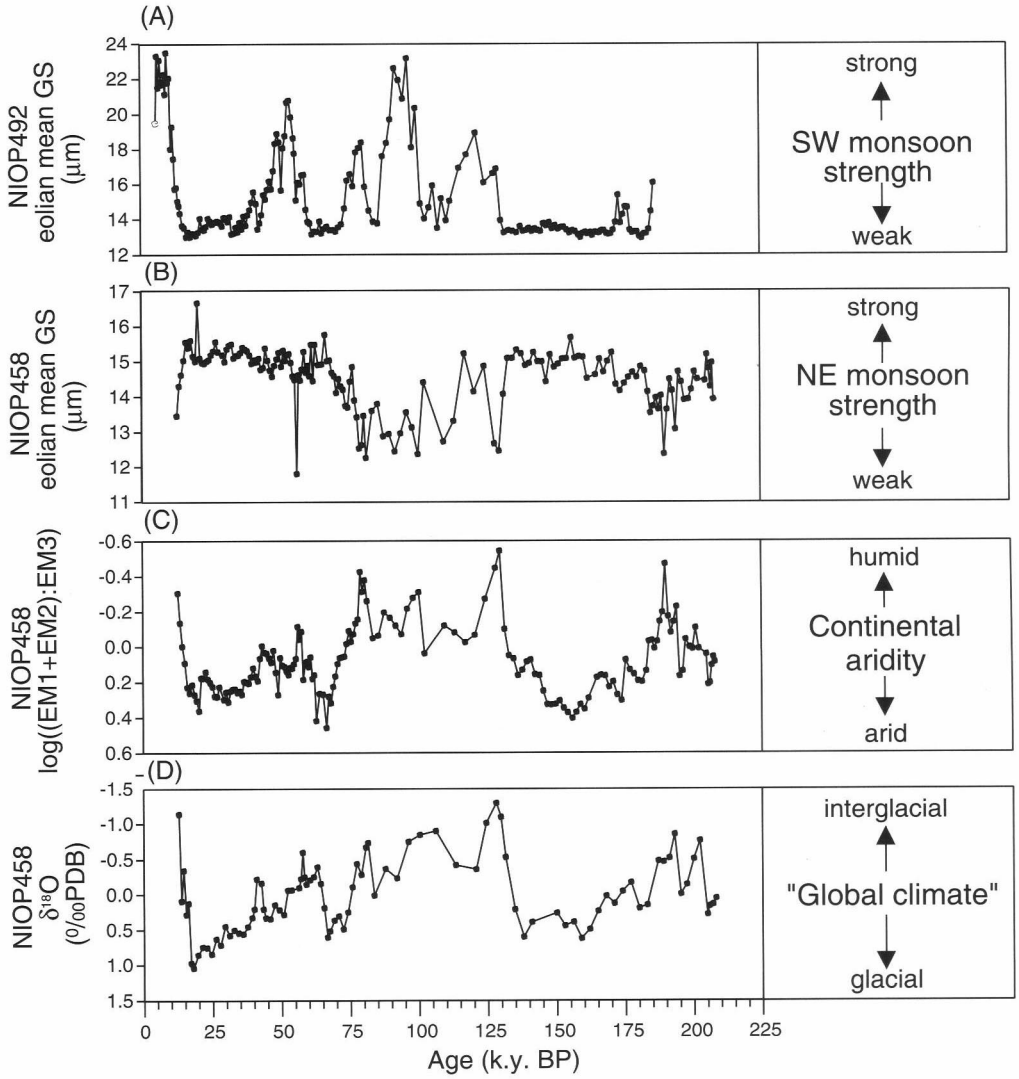

FIG. 17.—Late Quaternary reconstruction of variations in Arabian Sea monsoon climate. (A) Summer monsoon strength indicated by the eolian grain-size record of NIOP492. (B) Winter monsoon strength indicated by the eolian grain-size record of NIOP458. (C) Continental aridity indicated by log((EM1 + EM2):EM3) record of NIOP458. (D) "Global climate" indicated by $\delta^{18}O$ (*N. dutertrei*) record of NIOP458.

The eolian dust grain-size records from the Owen Ridge (NIOP492) and the upper Indus Fan (NIOP458) are inversely correlated. This apparent contradiction may be resolved by taking into account the characteristics of the present-day monsoon climate. The seasonal reversing atmospheric circulation pattern causes differences in the timing of eolian dust supply from the Arabian and Pakistan-Indian peninsulas that are the main source areas for the eolian dust deposited at sites NIOP492 and NIOP458. In the western Arabian Sea, the bulk of the eolian dust is deposited during the summer season (southwest monsoon), whereas in the northern Arabian Sea most of the eolian dust from the Pakistan-Indian deserts is supplied during winter (northeast monsoon). Taking this situation as a model for the late Quaternary, our data indicate that the southwest monsoon was stronger during interglacials (inferred from eolian dust record site NIOP492) and the northeast monsoon was stronger during glacials (inferred from eolian dust record site NIOP458). The good correlation between the eolian dust grain-size record of core NIOP492 and the (EM1 + EM2):EM3 record of core NIOP458 suggests a link between past variations in southwest monsoon intensity and continental aridity in the drainage basin of the Indus River.

Improvements of End-Member Modeling Over Descriptive Statistics

End-member modeling of grain-size distributions allows the distinction of subpopulations present within a basin fill. Such subpopulations may be related to different sediment sources or modes of transport (cf. Syvitski, 1991). Comparison of the grain-size records (Figure 14) from the Owen Ridge (NIOP492) and upper Indus Fan (NIOP458) illustrates clearly that the results of grain-size analyses of deep-sea sediments must be interpreted with great care. Variations in grain-size distributions in basin fills thus cannot be summarized with simple descriptive statistics such as the median or mean grain size if the objective of the study is to infer paleoclimate changes from the data.

The disadvantage of using descriptive statistics are illustrated for the three-end-member model developed in this study. Contour lines of mean and median grain size, sorting, and skewness (in ϕ) have been constructed in ternary diagrams for a range of mixtures of EM1, EM2, and EM3 (Figure 18A–D). As shown repeatedly in this study, variations in median size (or in any of the other grain-size statistics) cannot be interpreted unequivocally unless the grain-size distributions of the end members are known. For instance, a sediment with a mean grain size of 6.0 ϕ could be a mixture of 15% EM1 and 85% EM2, or a mixture of 57% EM1 and 43% EM3, or a mixture of varying proportions of all three end members. Additional information

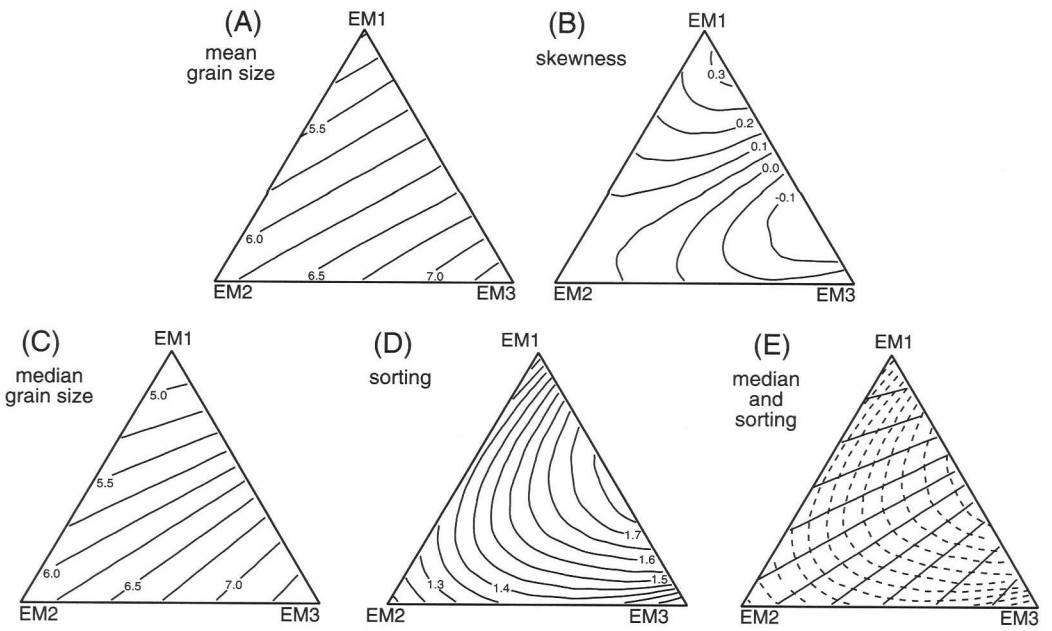

FIG. 18.—Contour plots of descriptive statistics (ϕ units) projected onto mixing space of the three-end-member model. (A) Mean grain size. (B) Skewness. (C) Median grain size. (D) Sorting. (E) Unique fingerprint is obtained by combining median (heavy lines) and sorting (dashed lines).

about the grain-size distribution is needed besides the mean grain size to fully characterize the sample. The location of each observation in the ternary mixing space can be uniquely defined by combining the median grain size and the sorting, as shown in Figure 18E; however, without the existence of the three-end-member model, these conclusions could not have been drawn.

DISCUSSION

Problems Associated with Proxies of Continental Aridity

The most widely used indicator of continental aridity is the flux of eolian dust. The construction of an eolian dust MAR record requires an age model of the sediment core, extraction of the terrigenous component, and extraction of the eolian dust component from the terrigenous component. The quality of the eolian dust flux record is highly dependent on the accuracy of each of these steps.

Age models of marine sediment records are normally based on the correlation of a limited number of age calibration points recognized in the $\delta^{18}O$ record with equivalent identifiable features on a orbitally based chronostratigraphy, in most cases the standard oxygen isotope records of Imbrie et al. (1984) or Martinson et al. (1987). Because the age model is based on relatively few calibration points, it produces only an approximate flux record. High-frequency variations in sediment flux occurring between two calibration points cannot be documented accurately.

In general, the distinction between the pelagic (eolian dust) and the hemipelagic (fluvial mud) terrigenous components is the most difficult and fundamental part of the problem associated with constructing eolian flux records. As shown in this study, end-member modeling of grain-size distributions allows such a distinction to be made, but the resulting eolian flux record still has limited use as a paleoclimatic indicator of continental aridity because it fails to capture high-frequency variations accurately.

The variations in weight percent of the terrigenous fraction observed by Clemens and Prell (1990, 1991), Shimmield et al. (1990), and Shimmield and Mowbray (1991) and the strong positive correlation between the terrigenous weight percent and magnetic susceptibility of sediments deposited on the Owen Ridge (Clemens and Prell, 1991) agree well with our observations on core NIOP492 (Figure 13B). Clemens and Prell (1991) suggested that the strong positive correlation between the terrigenous weight percent and magnetic susceptibility could be used to establish a terrigenous MAR. Under the assumption that the terrigenous fraction is of exclusive eolian origin, they proposed to use magnetic susceptibility as a high-resolution proxy for continental aridity; however, the terrigenous weight percent and magnetic susceptibility are both dependent on the ratio of carbonate and terrigenous MARs, which implies that they cannot be used as indicators of continental aridity.

Within core NIOP458 we see a relatively poor fit between terrigenous weight percent and magnetic susceptibility (Figure 13A). The poor fit may be attributed to early diagenetic processes that affected the redox stability of iron-bearing minerals and changed the magnetic properties of the sediment (Karlin and Levi, 1983). The alteration of the magnetic susceptibility records of sediment cores obtained from the oxygen-minimum zone off Pakistan and from the Murray Ridge has been related to oxidation of organic matter within these sediments (Reichart et al., 1994, 1997). Multiple terrigenous sources can further complicate the interpretation of the susceptibility signal. Especially when the input of hemipelagic mud is important, as in core NIOP458, both terrigenous weight percent and magnetic susceptibility lose their usefulness as indicators of continental aridity.

Linking Arabian Deep-Sea Records with Continental Records of the Chinese Loess Plateau

Several studies have suggested that the loess-paleosol sequences on the Loess Plateau of central China can be viewed as a proxy record of variations in Asian monsoon climate. The intensity of pedogenesis on the Loess Plateau is linked to summer monsoon precipitation. During pedogenesis, ultrafine-grained magnetite which is a highly susceptible mineral, is produced. The magnetic susceptibility of the loess-paleosol sequence thus is regarded as a proxy of summer monsoon strength (An et al., 1991). Several grain-size parameters of the loess have been used to reconstruct variations in strength of winter monsoon winds that were responsible for most of the dust transport (e.g., Ding et al., 1995; Porter and An, 1995; Xiao et al., 1995). Xiao et al.

(1995) concluded that winter monsoon strength, in general, is inversely related to the summer monsoon strength. On the Loess Plateau the summer monsoon intensified during stages 1, 3, 5, and 7 (An et al., 1991; Maher and Thompson, 1992), whereas the winter monsoon was strongest during stages 2, 4, and 6 (Xiao et al., 1995).

Clemens and Prell (1990) argued that the western Arabian Sea (Owen Ridge) lithogenic MAR record from core RC27-61 (dust source aridity indicator) and the magnetic susceptibility record from the Loess Plateau correlate well, from which they concluded the existence of a common aridity forcing mechanism. Maher and Thompson (1992) found only a general correspondence between the loess magnetic susceptibility record and their own lithogenic mass accumulation record at ODP site 722 (Owen Ridge). The discrepancy between the two records was explained by the fact that loess susceptibility records primarily reflect pedogenesis (formation of secondary magnetite), and to a much lesser extent the accumulation rate of the loess. In addition, they discussed the intrinsic problems of estimating accumulation rates of eolian dust in deep-sea cores. We fully support their conclusions. The problems associated with estimating accumulation rates have been discussed. The mass accumulation record presented by Clemens and Prell (1990) is difficult to interpret because they did not distinguish between eolian and hemipelagic sediments. The possible error associated with the assumption that the sediment is of exclusive eolian origin potentially refutes any correlation, as shown in this study.

The present-day monsoon precipitation on the Indian subcontinent and the associated continental runoff and sediment discharge by the Indus River are largely confined to the summer season (Beg, 1977; Nair et al., 1989), and therefore are coupled with the southwest monsoon. Based on this scenario, we propose that the (EM1 + EM2):EM3 ratio in core NIOP458, which depicts the relative importance of eolian dust transport with respect to lutite flow transport on the upper Indus Fan, may be used as an indicator of southwest monsoon intensity and thus also of continental runoff. The good correlation between the eolian grain-size record in core NIOP492 (Figure 17A), which can be related only to southwest monsoon strength, and the (EM1 + EM2):EM3 ratio of core NIOP458 (Figure 17C) supports this idea.

The (EM1 + EM2):EM3 ratio in core NIOP458 shows an excellent correlation with the oxygen isotope curve (compare Figure 17C and D), which allows us to infer that the late Quaternary history of continental runoff and summer monsoon intensity closely mimics the global oxygen isotope record of Imbrie et al. (1984). Maher and Thompson (1992) showed that the record of loess susceptibility closely fits the global oxygen isotope record of Imbrie et al. (1984). The late Quaternary history of pedogenesis and summer monsoon intensity on the Loess Plateau thus mimics the history of summer monsoon intensity in the area around the Arabian Sea. This suggests a physical connection between the regional summer monsoon patterns of the Arabian Sea and the Chinese Loess Plateau; i.e., the common aridity forcing mechanism postulated by Clemens and Prell (1990).

A physical connection between the regional winter monsoon patterns also can be established. The variations in northeast monsoon intensity, inferred from the eolian dust grain-size record of core NIOP458 (Figure 17B), indicate intensification of the winter monsoons during the glacial periods. This interpretation matches the conclusions of Xiao et al. (1995) with respect to intensity of the winter monsoon on the Loess Plateau. Additional support for intensified winter monsoons during the last glacial is provided by Duplessy (1982) on the basis of differences between the $\delta^{18}O$ ratios of planktonic foraminifera deposited during the last glacial maximum (18 k.y. BP) and the Holocene in the northern Indian Ocean.

In conclusion, our reconstruction of the late Quaternary monsoon climate, inferred from the grain-size distribution data of Arabian Sea sediments, corresponds well with paleoclimate reconstructions based on analysis of loess-paleosol sequences on the Loess Plateau of central China.

CONCLUSIONS

1. Detailed analysis of grain-size distributions in combination with the application of the end-member modeling algorithm allows the distinction of climate-induced changes of sediment-supply patterns in deep-marine depositional environments.
2. The siliciclastic fractions of the 1102 pelagic and hemipelagic mud samples from the western, northern, and central Arabian Sea are adequately described as mixtures of three end members. End-member modeling of grain-size distributions allows the distinction among coarse-grained eolian dust, fine-grained eolian dust, and fluvial mud.
3. The median grain-size records from the upper Indus Fan and the Owen Ridge are inversely correlated, reflecting contrasting sedimentation patterns in the two areas. Deposition on the Owen Ridge records selective transport and deposition of materials from a single source, whereas deposition on the upper Indus Fan records physical mixing of materials from two different sources (fluvial mud and eolian dust).
4. The grain-size distribution of eolian dust is calculated by subtracting the modeled contribution of the fluvial-mud end member from the grain-size distribution of the entire siliciclastic fraction.
5. The grain size of eolian dust is a high-resolution paleoclimatic indicator of wind strength.
6. Summer monsoon intensity is inversely correlated with winter monsoon intensity; an intensified southwest monsoon is recorded on the Owen Ridge during interglacials, whereas an intensified northeast monsoon is recorded on the upper Indus Fan during glacials.
7. The ratio of eolian and fluvial contributions in sediments of the upper Indus Fan is a high-resolution paleoclimatic indicator of continental aridity, which closely matches the marine oxygen isotope record. Increased continental aridity is recorded throughout the Arabian Sea during glacials.
8. The reconstructed variations in the Arabian Sea monsoon climate, inferred from grain-size distribution data, correlate well with the paleoclimate records of the Loess Plateau in central China. Physical connections between regional summer and winter monsoon patterns are established.

ACKNOWLEDGMENTS

We are indebted to all scientists, technicians, and crew members on board R.V. Tyro for their commitment during the Netherlands Indian Ocean Programme. We thank U. von Rad (BGR, Hannover, BRD), who kindly allowed us to sample the PAKOMIN core SO90-169KL. C. Laban (NITG-TNO, Haarlem) is thanked for his permission to use the GEOTEC multisensor core logger. We thank P. Anten, A. van Dijk, G. Ittman, M. Reith, G. vant' Veld, and H. de Waard for analytical support. J. Cleveringa, P. P. Lebbink, I. R. de Lugt, E. J. A. H. Noordhuis, G. J. Reichart, J.-B. W. Stuut, and H. J. Visser are thanked for their contributions, which comprise grain-size data, chemical analyses, magnetic susceptibility records, and a computer code for spline interpolation (not to mention a few wild ideas), for this study. We are especially grateful to G. J. Reichart, who kindly provided oxygen isotope and carbonate data, as well as age models of cores NIOP458 and NIOP464. P. L. de Boer, G. Ganssen, G. Postma,

J. B. W. Stuut, and M. E. Weber critically read the manuscript. We thank J. Harff, R. A. Olea, and an anonymous referee for their suggestions, which helped improve the manuscript. The investigations were in part supported by the Netherlands Geosciences Foundation (GOA), with financial aid from the Netherlands Organization for Scientific Research (NWO). This is Netherlands Research School of Sedimentary Geology (NSG) publication no. 970168.

REFERENCES

ALLEN, G. P., P. CASTAING, and A. KLINGEBIEL, 1971, Preliminary investigation of the surficial sediments in the Cap-Breton Canyon (southwest France) and the surrounding continental shelf: Marine Geology, v. 10, p. M27–M32.

ALLEN, G. P., P. CASTAING, and A. KLINGEBIEL, 1972, Distinction of elementary sand populations in the Gironde estuary (France) by R-mode factor analysis of grain size data: Sedimentology, v. 19, p. 21–35.

AN, Z., G. J. KUKLA, S. C. PORTER, and J. XIAO, 1991, Magnetic susceptibility evidence of monsoon variation on the Loess Plateau of central China during the last 130,000 years: Quaternary Research, v. 36, p. 29–36.

BEG, M. A. A., 1977, The Indus River basin and risk assessment of the irrigation system: International Working Seminar on Environmental Risk Assessment in an International Context, Tihanyi, Hungary, 13 p.

BRIDGE, J. S., 1981, Hydraulic interpretation of grain size distributions using a physical model for bedload transport: Journal of Sedimentary Petrology, v. 51, no. 4, p. 1109–1124.

CHAMBERS, R. L., and S. B. UPCHURCH, 1979, Multivariate analysis of sedimentary environments using grain size frequency distributions: Mathematical Geology, v. 11, no. 1, p. 27–43.

CLEMENS, S. C., and W. L. PRELL, 1990, Late Pleistocene variability of Arabian Sea summer monsoon winds and continental aridity: eolian records from the lithogenic component of deep-sea sediments: Paleoceanography, v. 5, no. 2, p. 109–145.

CLEMENS, S. C., and W. L. PRELL, 1991, One-million-year record of summer monsoon winds and continental aridity from the Owen Ridge (site 722), northwest Arabian Sea, *in* W. L. Prell, N. Niitsuma, et al., Proceedings of the Ocean Drilling Program, Scientific Results, v. 117, p. 365–388.

CLEMENS, S., W. PRELL, D. MURRAY, G. SHIMMIELD, and G. WEEDON, 1991, Forcing mechanisms of the Indian Ocean monsoon: Nature, v. 353, p. 720–725.

CURRAY, J. R., 1960, Tracing sediment masses by grain size modes: Report of the Twenty-First Session Norden, International Geological Congress, Copenhagen, p. 119–130.

DAL CIN, R., 1976, The use of factor analysis in determining beach erosion and accretion from grain size data: Marine Geology, v. 20, p. 95–116.

DAVIS, J. C., 1970, Information contained in sediment-size analyses: Mathematical Geology, v. 2, no. 2, p. 105–112.

DAVIS, J. C., 1986, Statistics and data analysis in geology (2d ed.): New York, John Wiley, 646 p.

DING, Z., T. LIU, N. W. RUTTER, Z. YU, Z. GUO, and R. ZHU, 1995, Ice-volume forcing of past east Asian winter monsoon variations in the past 800,000 years: Quaternary Research, v. 44, p. 149–159.

DOEGLAS, D. J., 1946, Interpretation of the results of mechanical analyses: Journal of Sedimentary Petrology, v. 16, no. 1, p. 19–40.

DOEGLAS, D. J., and W. C. BREZESINSKA SMITHUYSEN, 1941, De interpretatie van de resultaten van korrelgrootte-analysen: Geologie en Mijnbouw, v. 3, no. 8, p. 273–285; v. 3, no. 12, p. 291–302.

DOWLING, J. J., 1977, A grain size spectra map: Journal of Sedimentary Petrology, v. 47, p. 281–284.

DROZ, L., and G. BELLAICHE, 1991, Seismic facies and geologic evolution of the central portion of the Indus Fan., *in* P. Weimer and M. H. Link, eds., Seismic facies and sedimentary processes of submarine fans and turbidite systems: New York, Springer-Verlag, p. 383–402.

DUPLESSY, J. C., 1982, Glacial to interglacial contrasts in the northern Indian Ocean: Nature, v. 295, p. 494–498.

FILLON, R. H., and W. E. FULL, 1984, Grain size variations in North Atlantic noncarbonate sediments and sources of terrigenous components: Marine Geology, v. 59, p. 13–50.

FORREST, J., and N. R. CLARK, 1989, Characterizing grain size distributions: evaluation of a new approach using multivariate extension of entropy analysis: Sedimentology, v. 36, p. 711–722.

FULL, W. E., R. EHRLICH, AND J. E. KLOVAN, 1981, extended qmodel—objective definition of external end members in the analysis of mixtures: Mathematical Geology, v. 13, no. 4, p. 331–344.

FULL, W. E., R. EHRLICH, and J. C. BEZDEK, 1982, FUZZY QMODEL: a new approach for linear unmixing: Mathematical Geology, v. 14, no. 3, p. 259–270.

IMBRIE, J., J. D. HAYS, D. G. MARTINSON, A. MCINTYRE, A. C. MIX, J. J. MORLEY, N. G. PISIAS, W. L. PRELL, and N. J. SHACKLETON, 1984, The orbital theory of Pleistocene climate: support from a revised chronology of the marine $\delta^{18}O$ record, *in* A. Berger, J. Imbrie, J. Hays, G. Kukla, and B. Saltzman, eds., Milankovitch and climate, part 1: Dordrecht, Reidel, p. 269–305.

JÖRESKOG, K. G., J. E. KLOVAN, and R. A. REYMENT, 1976, Geological factor analysis: Amsterdam, Elsevier, 178 p.

KARLIN, R., and S. LEVI, 1983, Diagenesis of magnetic minerals in recent hemipelagic sediments: Nature, v. 303, p. 327–330.

KENYON, N. H., A. AMIR, and A. CRAMP, 1995, Geometry of the younger sediment bodies of the Indus Fan, *in* K. T. Pickering, R. N. Hiscott, N. H. Kenyon, F. Ricci Lucchi, and R. D. A. Smith, eds., Atlas of deep water environments: architectural style in turbidite systems: London, Chapman and Hall, p. 89–93.

KLOVAN, J. E., 1966, The use of factor analysis in determining depositional environments from grain size distributions: Journal of Sedimentary Petrology, v. 36, no. 1, p. 115–125.

KLOVAN, J. E., and A. T. MIESCH, 1976, EXTENDED CABFAC and QMODEL computer programs for Q-mode factor analysis of compositional data: Computers and Science, v. 1, p. 161–178.

KOLLA, V., and F. COUMES, 1987. Morphology, internal structure, seismic stratigraphy, and sedimentation on the Indus Fan: AAPG Bulletin, v. 71, p. 650–677.

KOLLA, V., and D. B. MACURDA, Jr., 1988, Sea-level changes and timing of turbidity-current events in deep-sea fan systems, *in* C. H. Wilgus, B. S. Hastings, H. Posamentier, J. Van Wagoner, C. A. Ross, and C. G. St. C. Kendall, eds., Sea-level changes—an integrated approach, *in* SEPM Special Publication 42, p. 381–392.

KOLLA, V., L. HENDERSON, and P. BISCAYE, 1976, Clay mineralogy and sedimentation in the western Indian Ocean: Deep-Sea Research, v. 23, p. 949–961.

KOOPMANN, B., 1981, Sedimentation von Saharastaub im subtropischen Nordatlantik während der letzten 25,000 Jahre: Meteor Forschungs-Ergebnisse, Reihe C, no. 35, p. 23–59.

KRISSEK, L. A., and S. C. CLEMENS, 1991, Mineralogic variations in a Pleistocene high-resolution eolian record from the Owen Ridge, western Arabian Sea (site 722): implications for sediment source conditions and monsoon history, *in* W. L. Prell, N. Niitsuma, et al., Proceedings of the Ocean Drilling Program, Scientific Results, v. 117, p. 197–214.

LIRER, L., and A. VINCI, 1991, Grain size distributions of pyroclastic deposits: Sedimentology, v. 38, p. 1075–1083.

LIRER, L., M. SHERIDAN, and A. VINCI, 1996, Deconvolution of pyroclastic grain size spectra for interpretation of transport mechanisms: an application to the A.D. 79 Vesuvio deposits: Sedimentology, v. 43, p. 913–926.

MAHER, B. A., and R. THOMPSON, 1992, Paleoclimatic significance of the mineral magnetic record of the Chinese loess and paleosols: Quaternary Research, v. 37, p. 155–170.

MARTINSON, D. G., N. G. PISIAS, J. D. HAYS, J. IMBRIE, T. C. MOORE, JR., and N. J. SHACKLETON, 1987, Age dating and the orbital theory of the ice ages: development of a high-resolution 0 to 300,000 year chronostratigraphy: Quaternary Research, v. 27, p. 1–29.

MCCAVE, I. N., 1972, Transport and escape of fine-grained sediment from shelf areas, *in* D. J. P. Swift, D. B. Duane, and O. H. Pilkey, eds., Shelf sediment transport: process and pattern: Stroudsburg, Pennsylvania, Dowden, Hutchinson and Ross, p. 225–248.

MCHARGUE, T. R., 1991, Seismic facies, processes, and evolution of Miocene inner fan channels, Indus submarine fan, *in* P. Weimer and M. H. Link, eds., Seismic facies and sedimentary processes of submarine fans and turbidite systems: New York, Springer-Verlag, p. 403–413.

MCHARGUE, T. R., and J. E. Webb, 1986, Internal geometry, seismic facies, and petroleum potential of canyons and inner fan channels of the inner Indus Submarine fan: AAPG Bulletin, v. 70, p. 161–180.

MIDDLETON, G. V., 1976, Hydraulic interpretation of sand size distributions: Journal of Geology, v. 84, p. 405–426.

MILLIMAN, J. D., G. S. QURAISHEE, and M. A. A. BEG, 1982, Sediment discharge from the Indus River to the ocean: past, present and future, *in* B. U. Haq and J. D. Milliman, eds., Marine geology and oceanography of Arabian Sea and coastal Pakistan: New York, Van Nostrand Reinhold, p. 65–70.

MURRAY, D. W., and W. L. PRELL, 1991, Pliocene to Pleistocene variations in calcium carbonate, organic carbon, and opal on the Owen Ridge, northern Arabian Sea, *in* W. L. Prell, N. Niitsuma, et al., Proceedings of the Ocean Drilling Program, Scientific Results, v. 117, p. 343–364.

NAIR, R. R., V. ITTEKKOT, S. J. MANGANINI, V. RAMASWAMY, B. HAAKE, E. T. DEGENS, B. N. DESAI, and S. HONJO, 1989, Increased particle flux to the deep ocean related to monsoons: Nature, v. 338, p. 749–751.

PORTER, S. C., and Z. AN, 1995, Correlation between climate events in the North Atlantic and China during the last glaciation: Nature, v. 375, p. 305–308.

PRINS, M. A., and G. POSTMA, 1997, Sea-level and climatic signatures in late Pleistocene–Holocene sediments of the Indus Fan (abs.): Terra Nova, Abstract Supplement 1, v. 9, p. 265.

REA, D. K., 1994, The paleoclimatic record provided by eolian deposition in the deep sea: the geologic history of wind: Reviews of Geophysics, v. 32, no. 2, p. 159–195.

REA, D. K., and S. A. HOVAN, 1995, Grain size distribution and depositional processes of the mineral component of abyssal sediments: Lessons from the North Pacific: Paleoceanography, v. 10, no. 2, p. 251–258.

REICHART, G. J., M. A. PRINS, and H. J. VISSER, 1994, Magnetic susceptibility, gamma ray transmissivity and XRF core-scanning, *in* W. J. M. Van der Linden and C. H. Van der Weijden, eds., Geological study of the Arabian Sea: Netherlands Indian Ocean Programme Cruise Report 3, Leiden, National Museum of Natural History, p. 97–115.

REICHART, G. J., L. J. LOURENS, and W. J. ZACHARIASSE, 1997, Orbital- and suborbital-controlled variability in the oxygen minimum zone (OMZ) of the northern Arabian Sea during the last 225,000 yr, *in* G. J. Reichart, ed., Late Quaternary variability of the Arabian Sea monsoon and oxygen minimum zone: Geologica Ultraiectina 154, p. 79-121.

REICHART, G. J., M. DEN DULK, H. J. VISSER, C. H. VAN DER WEIJDEN, and W. J. ZACHARIASSE, 1998, A 225-kyr record of dust supply, paleoproductivity and the oxygen minimum zone from the Murray Ridge (northern Arabian Sea): Palaeogeography, Palaeoclimatology, Palaeoecology, v. 134, p. 149–169.

RENNER, R. M., 1993, The resolution of a compositional dataset into mixtures of fixed source compositions: Applied Statistics, Journal of the Royal Statistical Society, v. 42, p. 615–631.

RENNER, R. M., 1995, The construction of extreme compositions: Mathematical Geology, v. 27, no. 4, p. 485–497.

SARNTHEIN, M., G. TETZLAFF, B. KOOPMANN, K. WOLTER, and U. PFLAUMANN, 1981, Glacial and interglacial wind regimes over the eastern subtropical Atlantic and northwest Africa: Nature, v. 293, no. 5829, p. 193–196.

SARNTHEIN, M., J. THIEDE, U. PFLAUMANN, H. ERLENKEUSER, D. FUTTERER, B. KOOPMANN, H. LANGE, and E. SEIBOLD, 1982, Atmospheric and oceanic circulation patterns off northwest Africa during the past 25 million years, *in* U. Von Rad, K. Hinz, M. Sarnthein, and E. Seibold, eds., Geology of the northwest African continental margin: Berlin, Springer-Verlag, p. 545–604.

SHERIDAN, M. F., K. H. WOHLETZ, and J. DEHN, 1987, Discrimination of grain size subpopulations in pyroclastic deposits: Geology, v. 15, p. 367–370.

SHIMMIELD, G. B., and S. R. MOWBRAY, 1991, The inorganic geochemical record of the northwest Arabian Sea: a history of productivity variation over the last 400 k.y. from sites 722 and 724, *in* W. L. Prell, N. Niitsuma, et al., Proceedings of the Ocean Drilling Program, Scientific Results, v. 117, p. 409–429.

SHIMMIELD, G. B., S. R. MOWBRAY, and G. P. WEEDON, 1990, A 350 ka history of the Indian Southwest Monsoon—evidence from deep-sea cores, northwest Arabian Sea: Transactions of the Royal Society of Edinburgh, Earth Sciences, v. 81, p. 289–299.

SIROCKO, F., 1991, Deep-sea sediments of the Arabian Sea: a paleoclimatic record of the southwest-Asian summer monsoon: Geologische Rundschau, v. 80, no. 3, p. 557–566.

SIROCKO, F., and H. LANGE, 1991, Clay-mineral accumulation rates in the Arabian Sea during the late Quaternary: Marine Geology, v. 97, p. 105–119.

SIROCKO, F., and M. SARNTHEIN, 1989, Wind-borne deposits in the northwestern Indian Ocean: record of Holocene sediments versus modern satellite data, *in* M. Leinen and M. Sarnthein, eds., Paleoclimatology and paleometeorology: modern and past patterns of global atmospheric transport: NATO ASI Series C 282, Dordrecht, Kluwer, p. 401–433.

SIROCKO, F., M. SARNTHEIN, H. LANGE, and H. ERLENKEUSER, 1991, Atmospheric summer circulation and coastal upwelling in the Arabian Sea during the Holocene and the last glaciation: Quaternary Research, v. 36, p. 72–93.

SIROCKO, F., M. SARNTHEIN, H. ERLENKEUSER, H. LANGE, M. ARNOLD, and J. C. DUPLESSY, 1993, Century-scale events in monsoonal climate over the past 24,000 years: Nature, v. 364, p. 322–324.

SOLOHUB, J. T., and J. E. KLOVAN, 1970, Evaluation of grain size parameters in lacustrine environments: Journal of Sedimentary Petrology, v. 40, no. 1, p. 81–101.

SYVITSKI, J. P. M., 1991, Factor analysis of size frequency distributions: significance of factor solutions based on simulation experiments, *in* J. P. M. Syvitski, ed., Principles, methods, and applications of particle size analysis: Cambridge, Cambridge University Press, p. 249–263.

TUREKIAN, K. K., and K. H. WEDEPOHL, 1961, Distribution of the elements in some major units of the earth's crust: GSA Bulletin, v. 72, p. 175–192.

VAN DER LINDEN, W. J. M., and C. H. VAN DER WEIJDEN, eds., 1994, Geological study of the Arabian Sea: Netherlands Indian Ocean Programme Cruise Report 3, Leiden, National Museum of Natural History, 136 p.

VISHER, G. S., 1969, Grain size distributions and depositional processes: Journal of Sedimentary Petrology, v. 39, no. 3, p. 1074–1106.

VAN DAM, J., and G. J. WELTJE, in press, Reconstruction of the late Miocene climate of Spain using rodent paleocommunity successors: an application of end-member modelling: Palaeogeography, Palaeoclimatology, Paleoecology.

VON RAD, U., and M. TAHIR, 1997, Late Quaternary sedimentation on the outer Indus shelf and slope (Pakistan): evidence from high-resolution seismic data and coring: Marine Geology, v. 138, p. 193–236.

Von Rad, U., H. Schulz, and Sonne 90 Scientific Party, 1995, Sampling the oxygen minimum zone off Pakistan: glacial-interglacial variations of anoxia and productivity (preliminary results, Sonne 90 cruise): Marine Geology, v. 125, p. 7–19.

Weltje, G. J., 1994, Provenance and dispersal of sand-sized sediments: reconstruction of dispersal patterns and sources of sand-sized sediments by means of inverse modeling techniques: Geologica Ultraiectina 121, 208 p.

WELTJE, G. J., 1995, Unravelling mixed provenance of coastal sands: the Po Delta and adjacent beaches of the northern Adriatic Sea as a test case, *in* M. N. Oti and G. Postma, eds., Geology of deltas: Rotterdam, Balkema, p. 181–202.

WELTJE, G. J., 1997a, End-member modeling of compositional data: numerical-statistical algorithms for solving the explicit mixing problem: Journal of Mathematical Geology, v. 29, p. 503–549.

WELTJE, G. J., 1997b, Construction of predictive regions in ternary diagrams: towards statistically rigorous provenance studies: Internal report with computer programs, Department of Geology, Faculty of Earth Sciences, Utrecht University, 28 p.

WOHLETZ, K. H., M. F. SHERIDAN, and W. K. BROWN, 1989, Particle size distributions and the sequential fragmentation/transport theory applied to volcanic ash: Journal of Geophysical Research, v. 94, no. B11, p. 15,703–15,721.

XIAO, J., S. C. PORTER, Z. AN, H. KUMAI, and S. YOSHIKAWA, 1995, Grain size of quartz as an indicator of winter monsoon strength on the Loess Plateau of central China during the last 130,000 yr: Quaternary Research, v. 43, p. 22–29.

ZHOU, D., H. CHEN, and Y. LOU, 1991, The log-ratio approach to the classification of modern sediments and sedimentary environments in northern South China Sea: Mathematical Geology, v. 23, p. 157–165.

ERRATUM

Prins and Weltje (1999), Figure 7C

(Prins, M. A., Weltje, G. J., 1999, End-member modeling of siliciclastic grain-size distributions: The late Quaternary record of eolian and fluvial sediment supply to the Arabian Sea and its paleoclimatic significance, *in* Harbaugh, J., et al., eds., Numerical experiments in stratigraphy: Recent advances in stratigraphic and sedimentologic computer simulations, SEPM (Society for Sedimentary Geology) Special Publication, v. 62, p. 91-111.)